Click Here for Full Article

Distinguishing high-alumina mare basalts using Clementine UVVIS and Lunar Prospector GRS data: Mare Moscoviense and Mare Nectaris

Georgiana Y. Kramer,[1,2] Bradley L. Jolliff,[3] and Clive R. Neal[1]

[1] High-alumina (HA) mare basalts are a unique group of the lunar sample collection. Sample geochemistry indicates that these basalts are derived from sources composed of late-stage cumulates from the Lunar Magma Ocean (LMO). Their aluminous nature suggests their sources contained significant plagioclase, which has implications regarding the efficiency of plagioclase separation from earlier forming, mafic cumulates in the LMO to form the anorthositic lunar crust, and hence the heterogeneity of the lunar mantle. The Apollo and Luna missions sampled HA basalts from four different locations that are separated by 80 equatorial degrees (~2400 km). Radiometric age dating of these samples demonstrates aluminous basaltic volcanism spanned over 1 billion years, suggesting HA basalts may be more prevalent on the Moon than implied by the sample population. Knowing their global occurrence would ultimately enhance our understanding of lunar evolution. Aluminous mare basalts occupy a unique location in Th-FeO compositional space that suggests they can be identified using global remote-sensing data of the Moon. We present our approach for distinguishing exposures of HA basalts using Clementine ultraviolet-visible-infrared (UVVIS) and Lunar Prospector Gamma Ray Spectrometer (LP-GRS) data with constraints based on the FeO, TiO_2, and Th abundances of Apollo and Luna HA samples. We identified 34 regions of interest (ROIs) where HA basalts could be a prominent component of the lunar surface. By analyzing the rims and proximal ejecta from small impacts (0.4–4 km in diameter) into the mare surface we characterized compositionally distinct basaltic units that make up the mare and thus determined which units represent HA basalt lavas. The results were used to generate maps that depict discrete mare units and classify their general basalt type. Here we focus on two ROIs: Mare Moscoviense and Mare Nectaris. Mare Moscoviense is composed of four basaltic units, two of which are HA candidates. Clementine UVVIS data of Mare Nectaris show evidence of up to three mare basalt units. One is the remnants of a mid-Ti unit that capped earlier low-Ti flows. The majority of the basin is filled by a compositionally indistinguishable low-Fe, low-Ti basalt. However, spectral profiles suggest there are two units. Regardless, the units both fit the criteria for a HA basalt.

1. Introduction

[2] The high-alumina (HA) mare basalts are a unique group of mare basalts among the variety of rock types returned by the Apollo and Soviet Luna missions [e.g., *Albee et al.*, 1972; *Grieve et al.*, 1972; *Helmke and Haskin*, 1972; *Ridley*, 1975; *Kurat et al.*, 1976; *Ma et al.*, 1979; *Shervais et al.*, 1985; *Dickinson et al.*, 1985; *Neal et al.*,

1988]. Their chemistry has implications for the nature of the mantle source from which they were derived and the evolution of the Lunar Magma Ocean [e.g., *Taylor and Jakes*, 1974; *Snyder et al.*, 1992; *Shearer and Papike*, 1999]. They have been sampled from widely separated locations on the lunar nearside (i.e., Apollo 14, Luna 16, and one sample from Apollo 12 and Apollo 16, each). Eruptions of these basalts pre-date and are contemporaneous with the extensive mare volcanism that filled the great lunar basins [e.g., *Dasch et al.*, 1987; *Nyquist and Shih*, 1992; *Snyder et al.*, 2000; *Cohen et al.*, 2001]. Their age range and variation in source chemistry suggests that HA basalts may not be uncommon, and could be related to cryptomare [*Hawke et al.*, 2005a, 2005b]. Learning their distribution can give us a better understanding of their

---

[1]Department of Civil Engineering and Geological Sciences, University of Notre Dame, Notre Dame, Indiana, USA.
[2]Now at Bear Fight Center, Winthrop, Washington, USA.
[3]Department of Earth and Planetary Sciences, Washington University, St. Louis, Missouri, USA.
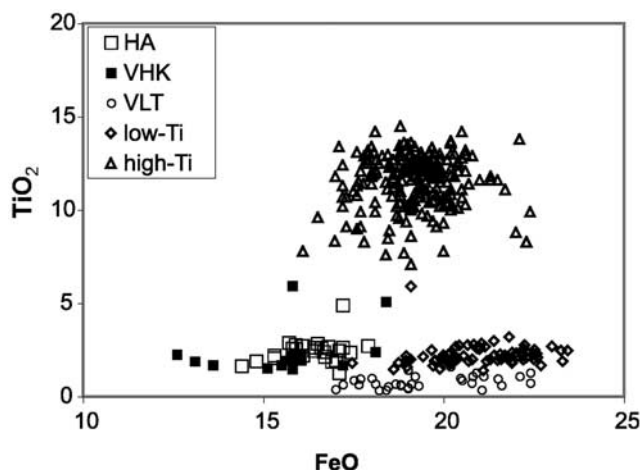
Figure 1. Wt% FeO versus wt% TiO_2 for mare basalts samples. Plot demonstrates the unique composition of HA basalts compared with other mare basalts, thereby allowing us to use remote-sensing data to locate new exposures. HA, high alumina; VHK, very high potassium; VLT, very low titanium. Data from C. R. Neal (Mare basalt database, Supplemental Material to New Views of the Moon, 2006).

volume and occurrence relative to other mare basalt types, which will help resolve mantle heterogeneity and the evolution of the Moon.

[3] The Clementine and Lunar Prospector (LP) missions provided compositional data that can be used to identify HA basalt compositions on the Moon. Remote-sensing instruments can only acquire information of the lunar surface; a regolith consisting of billions of years of physical weathering by solar wind and meteoritic bombardment. This process has mixed the lunar surface both laterally and vertically, which has tended to reduce lithologic contrast and obscure the composition of the bedrock. This mixing is particularly problematic, when searching for HA basalts, at contacts of high-FeO/low-Al_2O_3 mare basalts and low-FeO/high-Al_2O_3 highlands crust.

[4] There are two observations that motivated this research: (1) a plot of sampled mare basalt types demonstrates that HA basalts occupy a unique location in FeO versus TiO_2 space (Figure 1), and (2) a plot of global compositions from Lunar Prospector Gamma Ray Spectrometer (LP-GRS) (Figure 2a) shows a relatively high density of points (circled in black) in the region of intermediate FeO (13–17 wt%) and moderate to low Th (0.1–3 ppm), which is consistent with the compositions of HA samples (Figure 2b) when typical Fe offset differences of 2 wt% between soil and basalts are considered [*Basaltic Volcanism Study Project*, 1981; *Gillis et al.*, 2004]. In particular, their FeO concentrations are lower than most other mare basalts. Other basalts that plot in this space differ according to their Ti content (very low-Ti (VLT) basalts and some high-Ti basalts; see Figure 1). If the circled region in Figure 2a were the result solely of impact mixing between high-Fe, low-Th basalt and low-Fe-Th non-mare materials, one would expect a more even (linear) distribution. The higher density of points intimates that something else is contributing to the clustering.

[5] We present an approach that identifies potential HA basalt exposures on the lunar surface. We used LP-GRS thorium (0.5 degree/pixel) and Clementine-derived FeO and TiO_2 resampled to fit LP-GRS Th. Compositional parameters for a moon-wide search are based on known compositions from HA basalt samples and are used to map the distribution of HA basalts globally (Figure 3 and Table 1). The resulting regions of interest (ROIs) are more closely evaluated using high-resolution (100 m/pixel) FeO and TiO_2 compositional data from the Clementine multispectral camera. By looking at the rim and proximal ejecta of small impacts into the ROI, we can differentiate between mixtures of lithologies that mimic a HA basalt and a genuine HA exposure.

[6] In this paper we summarize current knowledge of the HA mare basalts, including their volcanic history and petrogenesis. As this research uses remote-sensing data, we present the relevant development and techniques utilized in our methods. Last we present our results for the analyses of Mare Moscoviense and Mare Nectaris.

2. Background

[7] The HA basalts are classified as mare basalts because they exhibit a mafic mineralogy with high FeO, high CaO/Al_2O_3 relative to the anorthositic highlands, and texture indicative of extrusive volcanism. Absolute and relative age
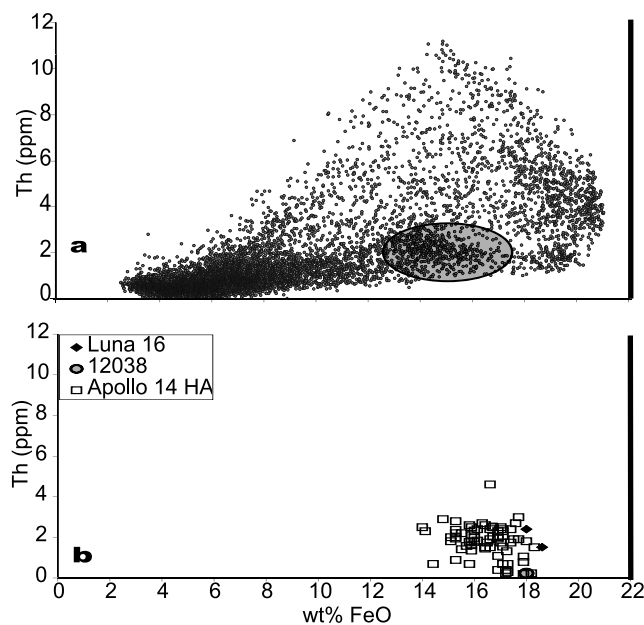
Figure 2. (a) Whole Moon remotely sensed FeO and Th from LP-GRS [*Lawrence et al.*, 2003; *Prettyman et al.*, 2002]; resolution is 2 degrees/pixel. Region circled highlights clustering of data points, which (almost) coincides with the range of HA compositions. (b) FeO versus Th concentrations measured in HA samples [*Brunfelt et al.*, 1972b; *Ma et al.*, 1979; *Shervais et al.*, 1985; *Dickinson et al.*, 1985; *Neal et al.*, 1988, 1989]. Offset of global remotely sensed HA basalts to 2 wt% lower FeO caused by dominance of lunar regolith by low-Ti highland lithologies.
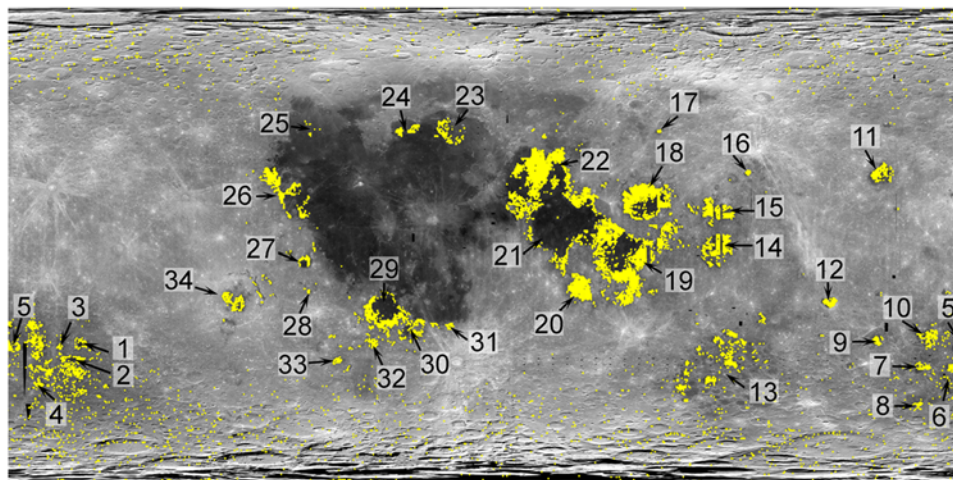
Figure 3. Clementine 750 nm base map at 1 km resolution. Yellow areas depict intersection of compositional constraints based on HA sample data: $12-18$ wt% FeO, $1-5$ wt% TiO_2, and $0-4$ ppm Th. FeO compositional data based on algorithms of *Lucey et al.* [2000a] and *Wilcox et al.* [2005] from Clementine data at 100 m/pixel. TiO_2 compositional data from algorithm of *Lucey et al.* [2000a] from Clementine data at 250 m/pixel. Th data from LP-GRS [*Prettyman et al.*, 2002] at half degree/pixel resolution. Numbers correspond to ROIs identified in Table 1.

dating demonstrate that aluminous volcanism postdates formation of the anorthositic lunar crust. These basalts are high in aluminum ($11-19$ wt% Al_2O_3) relative to other mare basalts ($7-11$ wt% Al_2O_3). Accompanying the high Al_2O_3 is a decrease in FeO (Figure 4), which corresponds to high modal proportions of plagioclase and lower pyroxene and olivine [cf. *Papike et al.*, 1974]. As is characteristic of all mare basalts, the HA basalts are variably enriched in trace elements relative to chondrites and have a negative Eu anomaly [e.g., *Shervais et al.*, 1985; *Neal et al.*, 1988; *Neal and Kramer*, 2006].

[8] Apollo 14 returned the greatest number of HA mare basalts. These came predominately in the form of clasts in breccia 14321 [e.g., *Grieve et al.*, 1975; *Duncan et al.*, 1975], although there are two HA specimens, not part of any breccia, 14053 and 14072 [*Papanastassiou and Wasserburg*, 1971; *El Goresy et al.*, 1972]. All of the Apollo 14 HA basalts are low-Ti ($1.5-4$ wt% TiO_2, Figure 5) and exhibit relatively minor variation in major element chemistry, which has been modeled by simple closed-system fractional crystallization [*Dickinson et al.*, 1985]. However, they vary substantially in their incompatible trace element abundance, demonstrating an eight-fold increase between the lowest and highest abundances. This complicates the matter of their petrogenesis, requiring a more complex explanation than simple fractional crystallization. Radiometric ages indicate at least three, and possibly four distinct ages ranging between $3.9-4.2$ Ga, which predate and are contiguous with low-alumina mare volcanism [*Papanastassiou and Wasserburg*, 1971; *Taylor et al.*, 1983; *Dasch et al.*, 1987; *Shih and Nyquist*, 1989a, 1989b]. Isotopic and trace element data are consistent with the age groups, indicating that the Apollo 14 HA basalts were derived from trace element distinct source regions at different times [*Neal and Kramer*, 2006].

[9] Only one sample from Apollo 12 is classified as HA (feldspathic group), 12038 [*Neal et al.*, 1994]. Because this basalt was the only one of its kind from this mission, it has

been suggested that 12038 is exotic to the Apollo 12 landing site [*Beaty et al.*, 1979]. It has also been suggested that it is native to the site, but comes from a stratigraphically deep layer of which only a small portion was excavated by crater impacts [*Nyquist et al.*, 1981]. Despite the proximity

**Table 1.** ROIs Highlighted by Compositional Constraints

|	ROI	Lat	Lon
1	Apollo (center)	36S	153W
2	Apollo (lower between rings)	43S	155W
3	Oppenheimer	46S	168W
4	Bose	55S	167W
5	Leibnitz	39S	179E
6	Von Karmen	46S	174E
7	Chretien	45S	161E
8	Poincaré	58S	162E
9	Jules Verne	35S	146E
10	Mare Ingenii	34S	168E
11	Mare Moscoviense	27N	146E
12	Tsiolkovskiy	20S	129E
13	Mare Australe (areas)	42S	90E
14	Mare Smythii	2N	89E
15	Mare Marginis	14N	87E
16	Lomonosov	28N	98E
17	Lacus Spei	43N	65E
18	Mare Crisium	18N	60E
19	Mare Fecunditatis	3S	51E
20	Mare Nectaris	16S	35E
21	Mare Tranquillitatis	9N	31E
22	Mare Serenitatis	25N	19E
23	South of Plato	43N	13W
24	Sinus Iridum	44N	30W
25	E. Sinus Roris	44N	64W
26	W. Proc (Struve)	20N	74W
27	Grimaldi	6S	68W
28	Cruger	17S	67W
29	Humorum	23S	40W
30	Palus Epidemiarum	31S	32W
31	Pitatus	30S	13W
32	Lacus Excellentiae	35S	42W
33	Lacus Excellentiae West	43S	56W
34	Mare Orientale	20S	95W
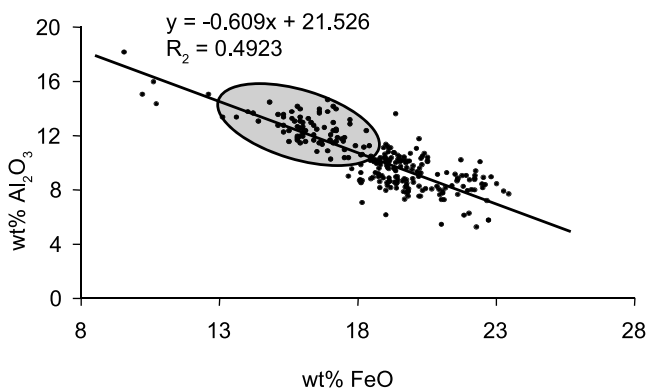
Figure 4. Inverse correlation of Al_2O_3 and FeO for mare basalt samples (the relationship does extend to highland samples) allows the use of FeO as a proxy for Al_2O_3 in the search for high-Al basalts using remote sensing. Circled region depicts HA mare basalts. Four lower-FeO data points are a subclass of HA basalts: the VHK basalts, not included due to their deviant characteristics. Data from C. R. Neal (Mare basalt database, Supplemental Material to New Views of the Moon, 2006).

of the two landing sites to each other, 12038's crystallization age of ~3.4 Ga precludes a relationship to any of the HA basalts from Apollo 14.

[10] Of all the Apollo missions, Apollo 16 landed the furthest from the maria (Figure 6) in the Cayley Plains. The mission did sample mare basalt fragments, all of which are considered exotic to the site, that is they were transported as ejecta from the surrounding maria [*Zeigler et al.*, 2006]. Of these basalt fragments only one was comparable to a HA basalt (60053,2-9 [*Zeigler et al.*, 2006]). 60053,2-9 resembles an Apollo 14 HA basalt in several aspects including
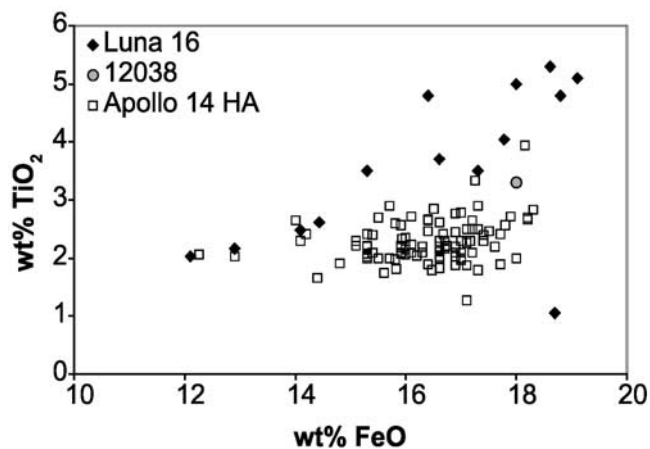
Figure 5. Wt% FeO versus wt% TiO_2 for HA mare basalt samples. Data sources: Luna 16: *Jakes et al.* [1972], *Kurat et al.* [1976], *Ma et al.* [1979]; Apollo 12: *Reid and Jakes* [1974]; Apollo 14: *Ehmann et al.* [1972], *Hubbard et al.* [1972b], *Lindstrom et al.* [1972], *Longhi et al.* [1972], *Strasheim et al.* [1972], *Taylor et al.* [1972], *Ridley* [1975], *Shervais et al.* [1985], *Dickinson et al.* [1985]; *Neal et al.* [1988, 1989], *Neal and Taylor* [1989].
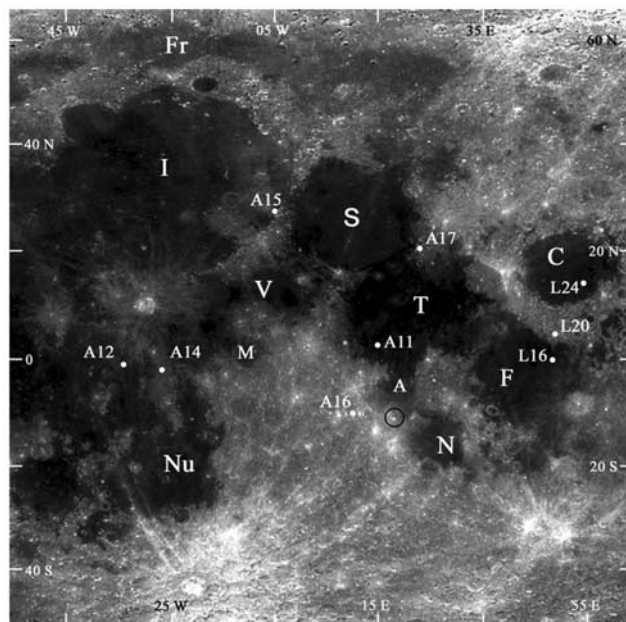

Figure 6. Simple cylindrical projection of a Clementine 750 nm image composite showing much of the lunar nearside. The sample return sites are labeled (A11, Apollo 11; L16, Luna 16; etc.), as well as some of the major mare filled basins (I, Imbrium; S, Serenitatis; N, Nectaris; T, Tranquillitatis; F, Fecunditatis; C, Crisium; Nu, Nubium; V, Vaporum; Fr, Frigoris; M, Sinus Medii; A, Sinus Asperitatis). The black circle approximates the rim of the 100 km crater Theophilus. From *Zeigler et al.* [2006].

mineral assemblage, texture, and mineral composition [*Shervais et al.*, 1985; *Longhi et al.*, 1972; *Taylor et al.*, 1983]. Its chondrite-normalized profile parallels the Apollo 14 basalts with the lowest incompatible trace element HA basalts, although with slightly greater absolute concentrations (Figure 7).

[11] Luna 16 returned a small drill core of the surface regolith composed of ~20% basaltic fragments [*Reid et al.*, 1972]. Virtually all of these basalts have a HA composition [*Kurat et al.*, 1976]. These samples have a greater variation in TiO_2 (1–5 wt%, Figure 5) and a lower Mg# (due to lower MgO) than Apollo 14 HA basalts [*Taylor et al.*, 1991]. Luna 16 HA basalts also exhibit a slightly bow-shaped chondrite-normalized rare earth element (REE) profile, whereas most Apollo 14 basalts are light rare earth element (LREE) enriched to varying degrees. Radiometric ages of the Luna 16 basalts suggest they are young (~3.15–3.5 Ga) relative to Apollo 14 HA basalts [*Huneke et al.*, 1972; *Cadogen and Turner*, 1977; *Fernandes et al.*, 2000; *Cohen et al.*, 2001] and erupted contemporaneously with other, low-alumina mare basalts. The unique chemistry and proportions of particle types in the Luna 16 regolith sample suggests the source material was derived from local areas [*Hubbard et al.*, 1972a], and thus implies that at least a portion of Mare Fecunditatis is dominated by aluminous mare basalts.

[12] It has been demonstrated that remotely sensed data from the Moon can be used to characterize different lunar terrains [*Jolliff et al.*, 2000], distinguish discrete mare basalt types [*Pieters*, 1978; *Pieters et al.*, 1995; *Hiesinger et al.*,
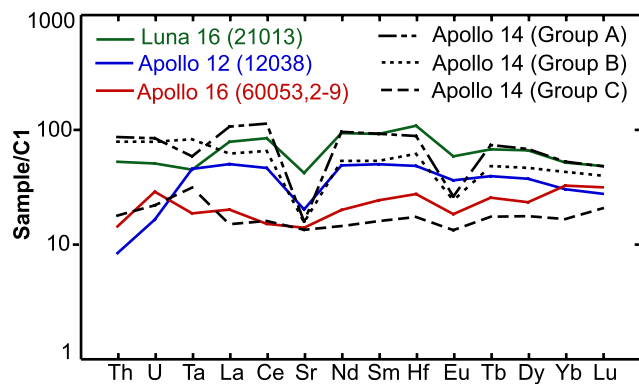
Figure 7. Chondrite-normalized trace element profile of HA mare basalts. X axis is trace element with decreasing incompatibility from left to right. Line pattern reflects parental compositions and mineral fractionation in the magma. Groups A, B, and C represent an average composition for each group as defined by *Neal and Kramer* [2006]. Luna 16 data are an average of compositions for sample 21003 from *Ma et al.* [1979]. Apollo 12 sample 12038 data from *Brunfelt et al.* [1972a]. Apollo 16 data from *Zeigler et al.* [2006].

1996; *Merenyi et al.*, 1997; *Gillis and Spudis*, 2000; *Staid and Pieters*, 2000], quantify the degree of cross-contamination between adjacent different terrains [*Mustard and Head*, 1996; *Staid et al.*, 1996; *Li and Mustard*, 2000, 2003], and measure the maturity of the regolith [*Fischer and Pieters*, 1994, 1996; *Shkuratov et al.*, 1999; *Lucey et al.*, 2000a]. Although several versions of lunar maps describing geology and morphology have been produced over the years, some regions based on telescopic data and some using remote-sensing data from Clementine [*Nozette et al.*, 1994] and Lunar Prospector [*Lawrence et al.*, 1998], this work presents the first attempt to locate specifically HA mare basalts and map basaltic units containing HA candidates. Our work will help identify the global distribution of this unique type basalt that previously has only been identified as small samples. This is particularly important for understanding lunar mantle dynamics due to the relationship between basalt chemistry and the evolving LMO.

3. Methods

[13] Our approach used three compositional parameters: FeO, TiO_2, and Th as these data are available at relatively high spatial resolution (half degree/pixel for Th with LP-GRS, and 100 m/pixel for Clementine-derived FeO and TiO_2). Incorporating MgO and Al_2O_3 would certainly be ideal, however current remote-sensing data for these oxides have a resolution no better than 5 degrees per pixel [*Feldman et al.*, 1999]. Distinguishing mare-highland mixtures from surfaces underlain by aluminous basalts, and particularly discerning different mare basalt types that fill a basin, is not practical at this resolution. Fortunately, the inverse correlation between FeO and Al_2O_3 makes it possible to use FeO as a proxy (Figure 4).

[14] The grouping identified in Figure 2a, which represents remotely sensed data, is shifted to lower FeO concen-

trations by approximately 2 wt% compared to Figure 2b, which represents sample data. There are two reasons for this: First, Figure 2b was created from sample data for which both FeO and Th measurements were taken. Although HA basalts have been measured with FeO abun-
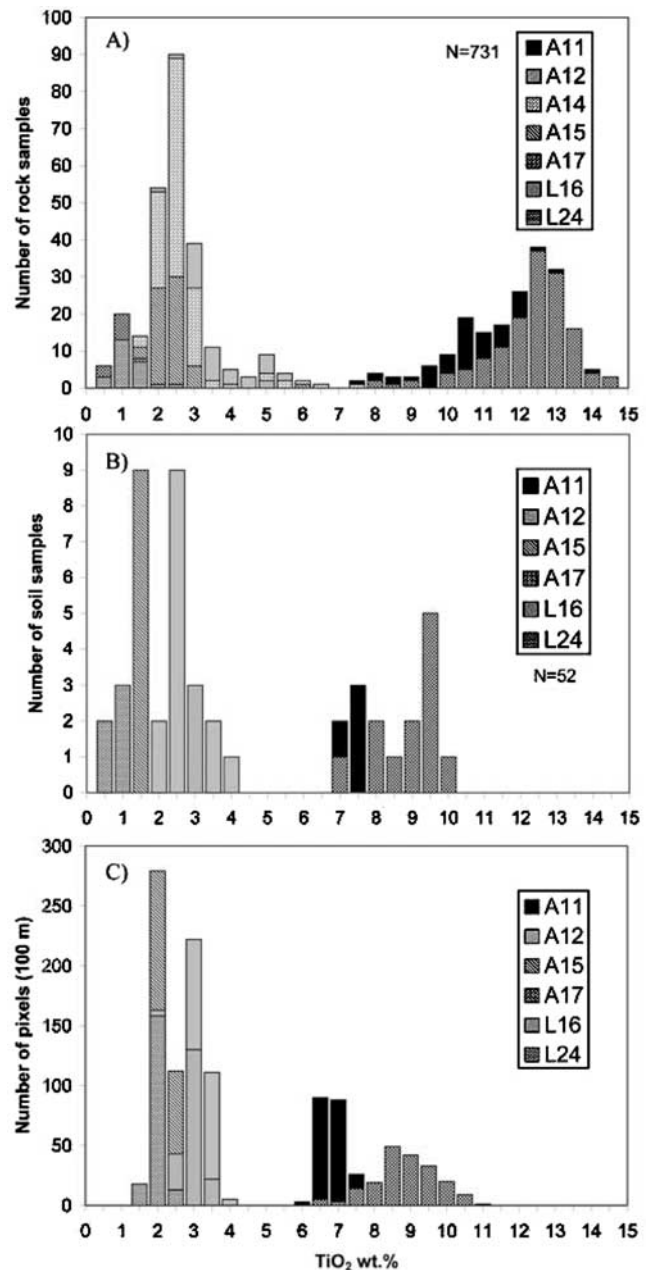
Figure 8. From *Gillis et al.* [2003]: (a) Histogram of TiO_2 concentrations for Apollo and Luna mare basalt samples. Note the "gap" in TiO_2 concentration between 5.5 and 9 wt% TiO_2. Data from *Basaltic Volcanism Study Project* [1981] and *Papike et al.* [1998]. (b) Histogram of TiO_2 concentrations determined for representative basaltic soils from individual Apollo (A) and Luna (L) sampling sites. (c) Frequency of Clementine UVVIS-based TiO_2 estimates determined using the modified regression for a 20×20 pixel image (100 m/pixel) that contains the respective landing site.
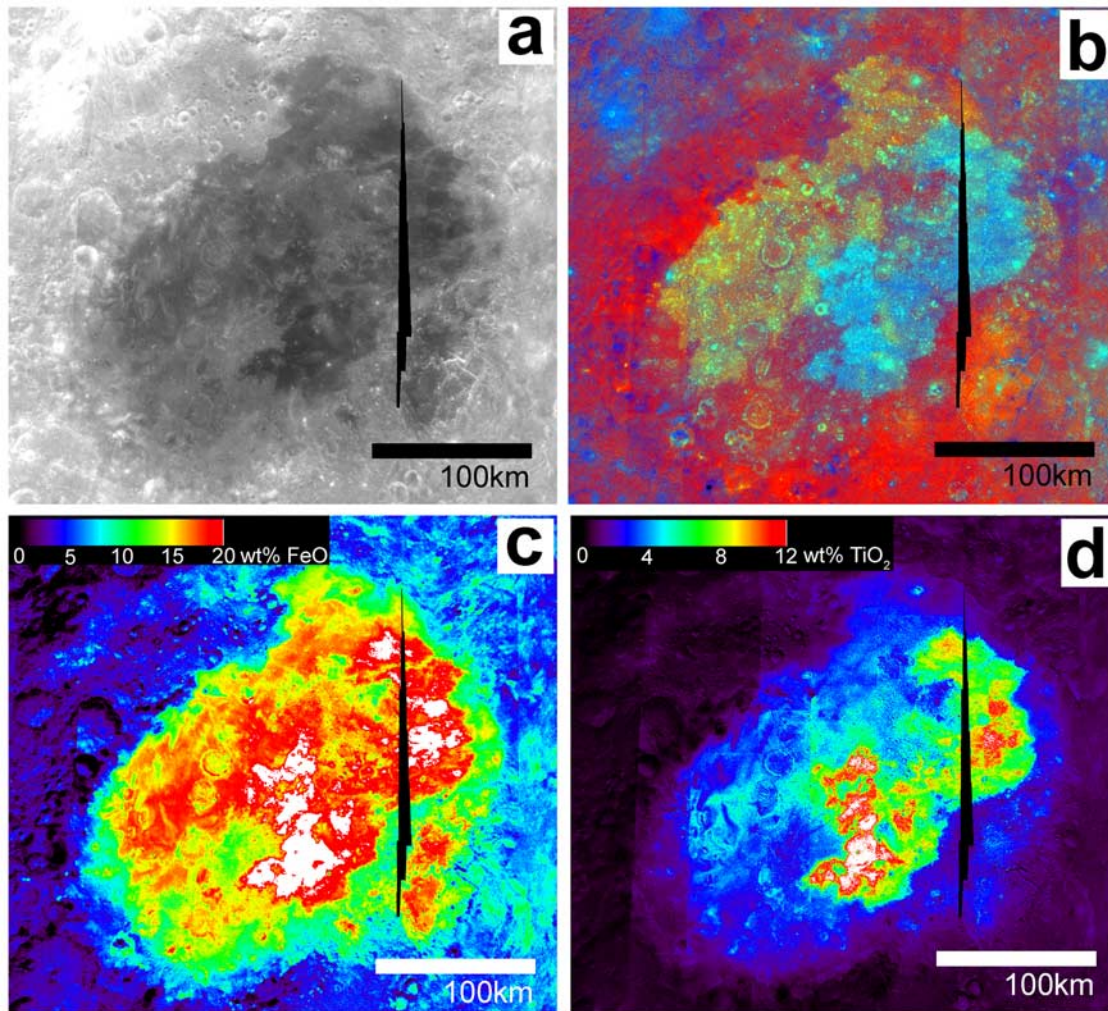
Figure 9. Clementine imagery for Mare Moscoviense: (a) 750 nm reflectance, (b) ratio, (c) FeO, and (d) TiO_2.

dances as low as 12 wt%, analyses that included Th coincidentally do not yield lower than 14 wt% FeO. Second, even the broad expanses of mare basalt flows on the Moon have non-mare materials mixed into the surface regolith, and because the lunar surface is dominated by low-FeO anorthositic highlands the FeO abundance of the regolith is always somewhat lower than that of the underlying basalts [*Gillis et al.*, 2004]. Our methods take this phenomenon into consideration. It is not necessary to shift the TiO_2 or Th parameters to compensate for the influence of the highlands on regolith composition. Both highlands and HA basalts have low-Ti and low-Th, so would not deviate significantly as is the case for FeO. This is demonstrated for TiO_2 in Figure 8. Although there are a handful of aluminous samples with TiO_2 values that slightly exceed 5 wt%, we truncated the whole Moon search at 5 wt% to account for the influence that low-Ti highland rocks would have on the soil composition overlying these basalts.

[15] We searched the whole Moon for regions that have a surface composition consistent with the composition of a HA basalt, as known from sample data. Specifically, we looked for those regions of the Moon where HA basalts dominate the regolith (>70%): FeO = 12–18 wt%, TiO_2 =

1–5 wt%, Th = 0–4 ppm. LP-GRS whole-Moon thorium data was fitted to Clementine simple cylindrical projection, and Clementine data was resampled to 0.5 degree per pixel resolution so the three data sets matched. We used the imaging software program ENVI (Environment for Visualizing Images) to create a filter that passed the intersection of these three compositional parameters (Figure 3). 34 regions of interest meet these constraints (Table 1).

4. Data and Processing

[16] High-resolution (100 m/pixel) Clementine UVVIS images of these ROIs were processed and calibrated using Integrated Software for Imaging Spectrometers (ISIS) [*Eliason*, 1997] from data available through Planetary Data Systems (PDS) [*Eliason et al.*, 1999] (Figures 9 and 10). The 750 nm reflectance image (Figures 9a and 10a) served as a monochrome base image to identify geomorphic and albedo features. However, where available, we incorporated Lunar Orbiter high-resolution images to aid with morphological identification and interpretation. We resampled all UVVIS channels to 100 m/pixel for this analysis. The ratio image (Figures 9b and 10b) is a color composite image
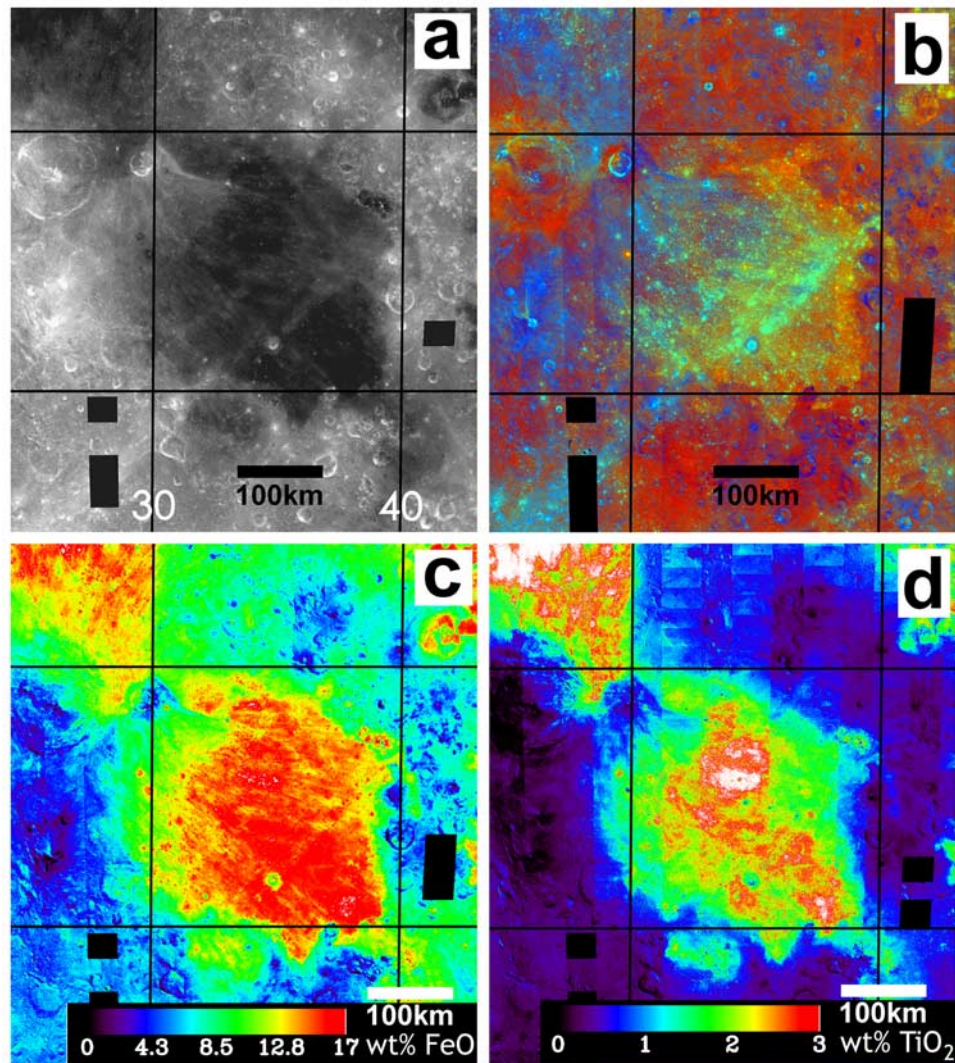
Figure 10. Clementine imagery for Mare Nectaris: (a) 750 nm reflectance, (b) ratio, (c) FeO, and (d) TiO_2.

(RGB) where each color depicts the ratio of two UVVIS bands. These three ratios reveal particular traits about the surface: The red channel contains the 750/415-nm ratio, which is sensitive to pyroclastic glass or mature highlands, characterized by an increasing VIS reflectance slope indicating the presence of nanophase Fe^0 and agglutinates produced by space weathering [*McCord and Adams*, 1973; *McKay et al.*, 1991; *Taylor et al.*, 2001; *Hawke et al.*, 2001]. The green channel is the 750/950-nm ratio, which reflects the amount of Fe^{2+} in minerals and glasses. Absorption of the 950 nm wavelength is caused by the presence of ferrous iron [*Burns*, 1982]; thus green is enhanced as the amount of FeO in a region increases (attributed to mare basalts). The blue channel is the 415/750-nm ratio, the value of which correlates positively with the abundance of ilmenite [*Charette et al.*, 1974], the dominant opaque mineral in most lunar basalts [e.g., *Papike et al.*, 1974]. Immature regolith also influences this channel because it has a lower abundance of agglutinates and nanophase Fe^0, and hence a shallower UVVIS slope. Blue in the image represents basalts with high TiO_2 concentra-

tions and fresh highland exposures. The ratio images provide clear distinctions between basalt units of sufficiently different compositions (Figure 9b), pyroclastic and/or impact melt, ejecta rays (Figure 10b) and swirl material.

[17] The FeO (Figures 9c and 10c) and TiO_2 (Figures 9d and 10d) compositional images were created on the basis of
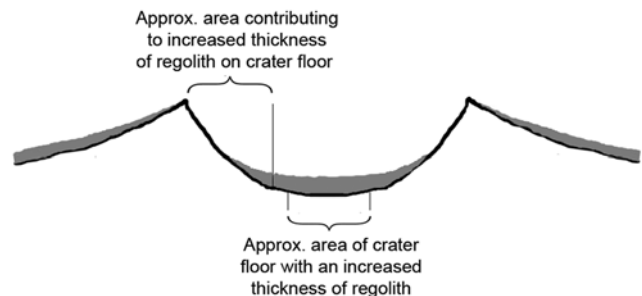
Figure 11. Schematic cross section of an impact crater demonstrating regolith deposition and buildup at crater floor.

the algorithms of *Lucey et al.* [2000b] (FeO < 10 wt%, TiO$_2$) and *Wilcox et al.* [2005] (FeO >10 wt%). We logged the FeO and TiO$_2$ abundances from the pixel values of the rim and proximal ejecta of small (0.4−5 km) impacts into each ROI. Such impacts are large enough to punch through the surface regolith, and yet small enough not to completely penetrate the mare basalt flows. In this way, the impacts act as windows through the regolith, exposing the composition of the underlying basalt [*Staid and Pieters*, 2000].

[18] We generated an optical maturity index (OMAT) [*Lucey et al.*, 2000a; *Wilcox et al.*, 2005] image of each ROI and at the same resolution to ensure the measurement of fresh craters. The pixels from which we are extracting basalt compositions depict crater ejecta that impacted into mare basalts, and therefore have FeO abundances greater than 10 wt%. Above 10 wt% FeO the *Lucey et al.* [2000a] method does not give reliable maturity and iron values with which to distinguish mare basalt units [*Wilcox et al.*, 2005]. We therefore used the *Wilcox et al.* [2005] algorithms for FeO and OMAT, which give more consistent results. Values for OMAT parameters range from −1.05 to −0.65, with values increasing with increasing maturity [*Wilcox et al.*, 2005]. OMAT values <−0.92 were used only when an area did not contain a representative number of craters with values >−0.92. Practically, the craters we analyzed were largely no better than −0.8. These values are rather mature with respect to the range of possible values, however, they represent the least mature values available in the ROI.

[19] The compositions from Clementine-derived data will appear to vary significantly within and around a single crater. Small scale variations related to slope are strongly affected by lighting geometry in known ways [*Jolliff*, 1999]. To minimize these effects measurements on each crater were taken from no less than 20 (and up to 150) points on the crater rim and into the proximal ejecta. The average of the data points is taken to be the closest approach to the composition of the mare basalt unit exposed in that location and depth (∼1/10 the diameter of the crater).

[20] In an effort to mitigate the inherent problem of relating sample compositions to remotely sensed data on an airless, geologically inactive planetary body, we extracted spectral information from the crater rim and proximal ejecta of the least mature craters. The ubiquitous regolith is composed mostly of underlying and immediately adjacent lithologies, but also contains a significant fraction of material from more exotic locations. The contribution of exotic materials to a given location increases with increased maturity of the location. The crater floor, which represents the greatest depth of penetration, has previously been used for extracting compositional information [*Staid and Pieters*, 2000]. However, we consider this area to not be an ideal location as it would be covered with regolith produced since excavation, as would any flat region of the lunar surface, plus material that cannot deposit on the crater wall due to its slope exceeding the angle of repose (Figure 11).

[21] The crater wall would seem the next logical surface to analyze, unfortunately reflectance data suffer from variations in albedo caused by the same steep angles that prevent material from depositing on it [*Jolliff*, 1999]. While the slopes of the rim and proximal ejecta are not usually steep enough to slough off all unconsolidated material, they may prevent the degree of regolith buildup as would occur

on a flat surface. The slopes are certainly not so steep as to introduce erroneous spectral information due to lighting geometry. More importantly, impact cratering studies and analysis of impact ejecta mechanics demonstrate that near the crater rim the original stratigraphy of the impact target is inverted [e.g., *Melosh*, 1989]. Therefore collecting data from this region provides the best approach to the composition of the underlying basaltic unit. Despite these efforts to obtain the most accurate values possible, contamination from adjacent units, and the effects of space weathering, still influence the composition of the regolith. These factors are taken into consideration in our final characterization of each unit.

[22] For this paper, our analysis focused on two ROIs and produced mare basalt unit maps for each of Mare Moscoviense and Mare Nectaris (Figures 12 and Figure 13). We analyzed Mare Moscoviense first because the ratio image (Figure 9b) shows a brilliant separation of the basalt units, aiding in the analysis. The conclusion of *Zeigler et al.* [2006] on the source of HA basalt regolith fragments from Apollo 16 prompted the selection of Mare Nectaris.

5. Discussion

5.1. Mare Moscoviense

[23] There are four basaltic units filling Moscoviense basin (Figure 12): (1) Im, an Early(?) Imbrian, very low-Ti, low-Fe basalt; (2) Iltm, an Imbrian-age, low-Ti, mare basalt; (3) Ikm, an Imbrian low-Ti basalt that partially fills
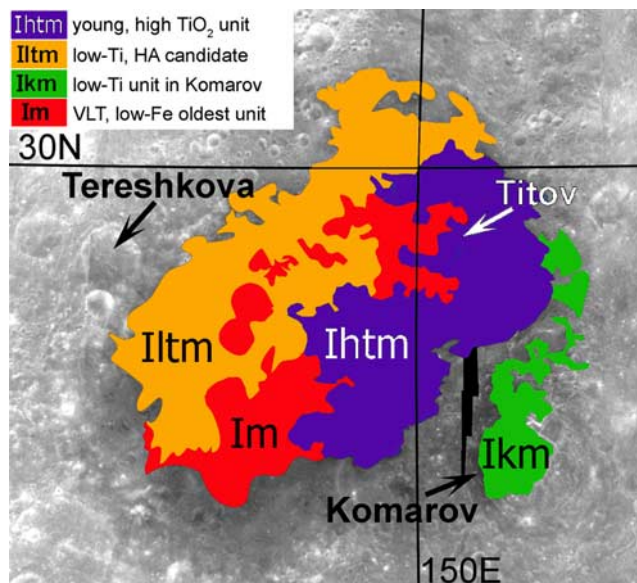
Figure 12. Mare basalt unit map of Mare Moscoviense. The base map was constructed using Clementine 750 nm at 100 m/pixel. The map depicts the multiple basalt flows that fill the basin. *Im* is the oldest unit and has a low-FeO, VLT composition that may be impact melt or a heavily battered basalt whose true composition is being obscured. *Ikm* may be a high-Al basalt, but the deposit is thin and may have a high-Al composition due to vertical mixing with the basin floor. *Iltm* has the composition of a high-Al basalt. *Ihtm* is a young, high-Ti basalt. Large craters labeled for reference points.
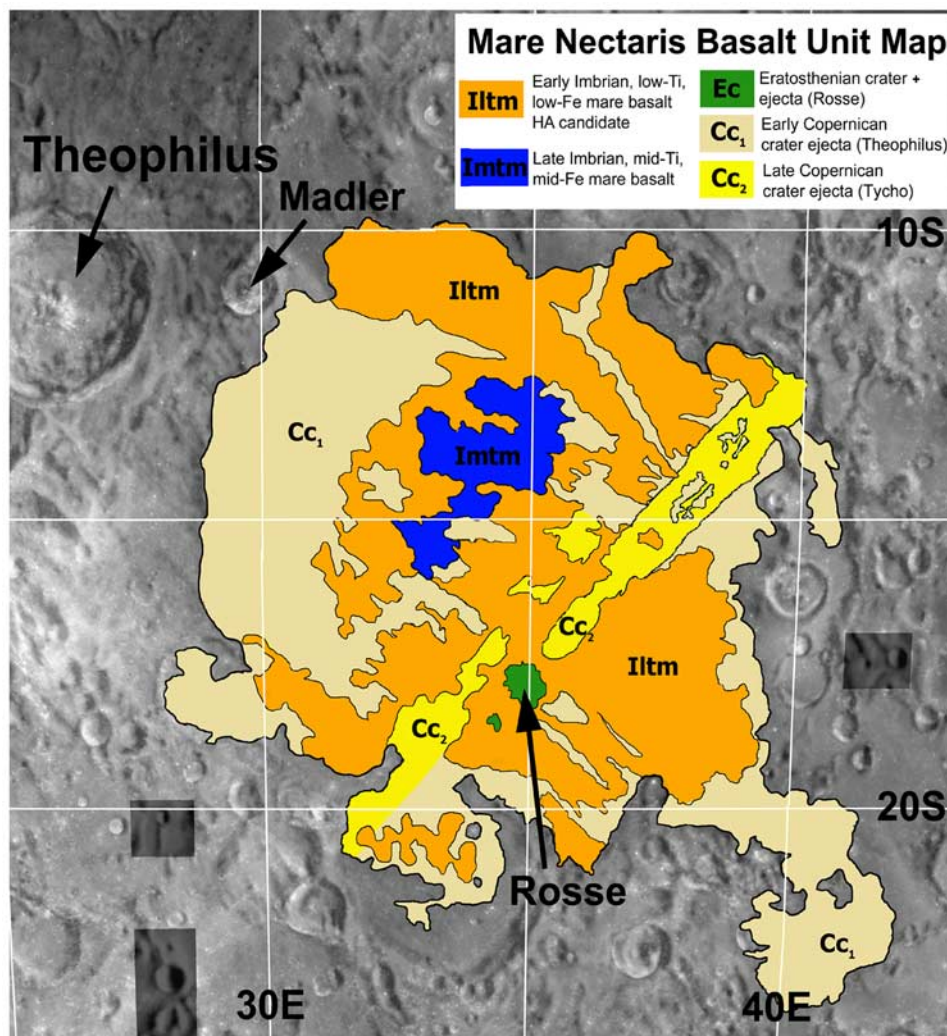
Figure 13. Mare basalt unit map of Mare Nectaris. Base map is derived from Clementine 750 nm at 125 m/pixel resolution. The map depicts one main mare-filling basalt unit and one mid-Ti unit that capped the mare. The anomalously high TiO_2 content of the surface regolith in this area is the only indication that this thin capping flow unit once existed. Craters of various sizes across the mare reveal similar compositions, implying that Mare Nectaris is dominated by one mare unit with the composition of a HA basalt. Also depicted are crater rays and ejecta deposits that obscure the basalt beneath them.

the crater Komarov; and (4) Ihtm, and a Late(?) Imbrian, mid- to high-Ti, high-Fe basalt. Since we identified the same units described by *Gillis* [1998], we used the same nomenclature and age relationships for unit designations. Unit boundaries and surface compositions are also consistent with *Craddock et al.* [1997]. In an effort to obtain a representative number of craters to define each basaltic unit, only those with OMAT parameters ≥ -0.98 were selected (Table 2). Values between -0.98 and -0.92 are plotted as open symbols and craters with OMAT parameters ≥ -0.92 as filled symbols in Figure 14. OMAT values < -0.92 were used only when an area did not contain a representative number of craters with values > -0.92. The units are described in detail below in order of oldest to youngest.

5.1.1. Unit Im

[24] The oldest unit, Im, has very low FeO (10−12 wt%) and low TiO_2 (1.75−2.25 wt%) as revealed by the small impacts (Figure 14). The unit is more extensive than

suggested by its exposure. Its composition is found in larger impacts into Unit Iltm. FeO abundances in excess of 12 wt% are correlated with more mature craters, and thus are interpreted as evidence of contamination by neighboring higher-Fe units. FeO concentrations are lower than is typical of a mare basalt, even of a HA basalt. *Craddock et al.* [1997] described the unit as a pyroclastic deposit, while *Gillis* [1998] described it as basaltic with a high glass content, and similar in composition to a Low Potassium Fra Mauro material. Considering the potential relationship of aluminous basalts and cryptomare [*Hawke et al.*, 2005a, 2005b], the early flows could be HA in composition. On this basis, one might conclude that this unit is a HA basalt. However, the characterization of this unit is difficult because it has experienced sufficient impact gardening to obscure its composition. Craters with favorable OMAT parameters do not exceed 1 km in diameter nor do their ejecta expose a composition that definitively reveals the

Table 2. Compositions and Maturity of Small Craters in Mare Moscoviense

	Im		Iltm		Ikm		Ihtm	
	FeO	TiO$_2$	FeO	TiO$_2$	FeO	TiO$_2$	FeO	TiO$_2$
			0.4−1 km Diameter					
OMAT >−0.92	9.38	2.13	10.94	1.19			16.1	3.69
	10.51	1.57	11.63	1.59			16.3	3.88
	11.34	1.76	13.29	2.04			13.4	3.56
	12.18	2.09	12.8	1.95			17.09	6.18
			13.12	0.83			17.39	5.74
			12.2	1.81			17.59	5.11
			14.06	1.93			18.35	7.67
			14.2	2.61			17	4.65
			15.22	3.04			16.39	4.39
			15.25	2.72				
			14.89	2.98				
			13.72	2.55				
			12.63	1.51				
			13.65	2.13				
			12.99	1.76				
			13.57	2.19				
			13.52	2.15				
			15.59	3.19				
			15.46	3.3				
			11.72	1.42				
			11.38	1.59				
			16.74	2.13				
OMAT −0.98 to −0.92	11.38	1.82	13.55	2.04	14.74	2	16.13	5.85
	10.32	2.15	15.24	2.46	14.45	2.08	17.93	7.65
	10.93	2.25	14.49	2.34	14.77	2.25	17.75	7.03
	10.75	2.27	14.87	2.99	15.48	1.95	18.17	8.233
	10.46	1.61	13.83	1.8	13.61	2.15	18.6	7.43
	12.47	2.09	15.57	3.58	14.05	1.85	18.91	7.96
	12.83	2.26	13.94	2.37			15.3	5.07
	12.2	1.81	12.63	2.27			18.08	8
	14.42	2.64	14.85	2.86			16.89	5.37
	10.12	1.74	11.88	1.16			13.54	3.63
	11.88	1.81	12.66	2.14			17.69	6.94
	13.23	1.57	13.61	2.14			15.9	5.42
	12.25	2.27	14.35	2.08			16.08	5
	12.02	1.49	14.03	2.01			16.8	5.71
	13.31	1.92	13.68	2.25			17.42	6.36
	13.36	1.75					14.34	3.52
	11.33	1.74					16.97	5.89
	11.69	2.45					17.56	6.81
	13.12	1.71					17.25	5.6
							13.51	3.9
							16.42	5.38
							15.22	4.5
							16.07	4.98
							15.71	4.28
							18.3	7.75
							17.24	7.33
							16.72	6.43
							16.29	5.44
							17.55	6.62
							17.63	6.08
			1−2 km Diameter					
OMAT >−0.92			11.07	1.33			16.08	4.49
			13.98	2.63			16.99	5.17
			13.07	1.54			16.47	5.42
			13.61	1.96			17.67	6.21
			11.85	1.33			11.03	2.77
			15.05	3.33				
OMAT −0.98 to −0.92			13.05	2.02	15.09	1.79	16.05	4.86
			15.1	3.16			16.37	5.02
			13.53	1.97			14.11	3.99
			14.7	2.59			17.85	6.17
			14.06	2.33			17.65	6.17
			13.35	1.64			16.24	5.76
			11.79	1.39			17.13	6.34
			11.94	1.25			18.19	7.88
			12.13	1.44			14.17	3.99
			13.25	1.87			17.83	6.82
			14.89	3.09				

Table 2. (continued)

	Im		Iltm		Ikm		Ihtm	
	FeO	TiO$_2$	FeO	TiO$_2$	FeO	TiO$_2$	FeO	TiO$_2$
			14.33	2.82				
			15.11	2.96				
			14.91	2.58				
			12.89	1.97				
			14.23	2.59				
			13.28	2.73				
			2−3 km Diameter					
OMAT −0.98 to −0.92			13.62	2.71				
			13.84	2.68				
			13.56	2.08				
			12.82	2.27				
			3−4 km Diameter					
OMAT −0.98 to −0.92			14.1	3.19				
			14.15	3.25				

basin floor, thereby precluding an estimation of the extent of contamination by vertical mixing. Furthermore, the unit's composition, as estimated from the few small impact craters are below the sample constraints for a HA basalt.

5.1.2. Unit Iltm

[25] Unit Iltm, on the northwestern half of Moscoviense, was the next unit to fill the basin and covered much of unit Im. Impacts into Unit Iltm reveal a wide range in FeO and TiO$_2$ abundances that give an idea of its lateral and vertical extent (Figure 14). The regolith atop this unit exhibits slightly higher FeO values than impacts into unit Iltm due to the influence of the adjacent higher iron unit, Ihtm, to the east. We thus estimated the composition of unit Iltm to be at the median and densest clustering of compositions apparent in Figure 14: 13−15 wt% FeO and 2−3.5 wt% TiO$_2$. As a result, Unit Iltm is an ideal candidate for a HA basalt exposure.

5.1.3. Unit Ikm

[26] Unit Ikm is a small mare basalt unit that partially fills the crater Komarov, which lies southeast of the main Mare Moscoviense flows. The mare and crater floor are crossed by several fissures, which expose low-Fe feldspathic highlands crust. The surface composition (∼14.25 wt% FeO, ∼2 wt% TiO$_2$) is intermediate between that of units Im and Iltm, however it is practically devoid of small, fresh impacts. This lack of craters prevented *Gillis* [1998] from estimating a relative age of unit Ikm, although he did consider it similar in age to Iltm. *Craddock et al.* [1997] mapped units Iltm and Ikm as a single unit they designated "red mare". Only six craters had OMAT parameters greater than −0.98, a rather mature value. From these craters we found the unit composition to be ∼14.8 wt% FeO and ∼2 wt% TiO$_2$. Ikm may be a HA basalt candidate; however, the lack of a more representative number of immature craters precludes a definitive designation.

5.1.4. Unit Ihtm

[27] The high-Ti, eastern basalt flow, Unit Ihtm, is the youngest of the four that fill Moscoviense. As described by *Gillis* [1998], and observed in our analysis, there are small impacts into Unit Ihtm the composition of which are consistent with the composition Iltm. This demonstrates that Ihtm has flowed over, and partially covered Iltm. Small craters in the unit reveal a wide range in compositions (Figure 14). However, lower-Fe and -Ti abundances are probably the result of contamination from units Im and Iltm due to impact mixing. There is no other apparent source of high-Ti in the vicinity that could influence the composition of the regolith besides this high-Ti unit itself. Therefore, we concluded that the composition of Unit Ihtm is best represented by the highest FeO and TiO$_2$ concentrations shown in Figure 14: 17−19 wt% FeO, 7−8.25 wt% TiO$_2$. These values clearly exceed the constraints for a HA basalt.

5.2. Mare Nectaris

[28] *Pieters* [1978] and *Wilhelms* [1987] mapped one unit filling Nectaris, while *Kodama and Yamagucji* [2003] identified two mare units: Nc1 and Nc2. The latter study acknowledged that the entire basin is filled with basalt flows
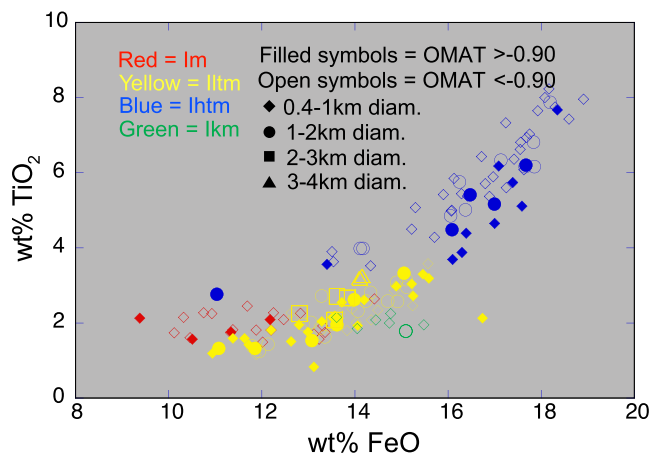
Figure 14. Composition of rims and proximal ejecta for small impacts into Mare Moscoviense. Each point represents the average of several pixel values for one impact. Unit designations after *Gillis* [1998]: *Im*, VLT mare basalt; *Iltm*, low-Ti mare basalt; *Ihtm*, high-Ti mare basalt; *Ikm*, low-Ti mare basalt filling Koramov. Color coding corresponds to impacts into these units. Symbols distinguish craters of varying size and OMAT parameter. There is a clear distinction between different units revealed by these impacts. Data from Clementine 100 m/pixel.
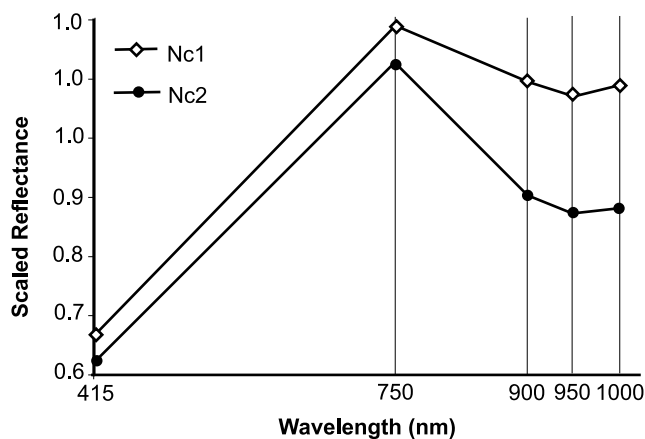
Figure 15. Spectral profiles of two units identified by *Kodama and Yamagucji* [2003] in Mare Nectaris. These spectra are taken from the surface (regolith) and are not the same ones that we identified from the ejecta of small impact craters (see Figure 16). From *Kodama and Yamagucji* [2003].

of a roughly uniform composition, yet divided the mare on the basis of two different surface spectra, describing Nc2 spectra as having a higher UV/VIS ratio and stronger 1 micron absorption than that of unit Nc1 (Figure 15). *Kodama and Yamagucji* [2003] based their geologic map of Nectaris on Clementine spectra of the surface. Thus their map represents the regolith composition and not the basalt composition that we worked to characterize using the composition of crater ejecta.

[29] Like Moscoviense, we determined mare basalt unit compositions by collecting spectral information from several small impact craters across Mare Nectaris ranging from 0.4 to 4 km in diameter, and that are relatively immature (Tables 3a and 3b). Unlike Moscoviense, Clementine composite images do not delineate clearly distinguishable mare basaltic units in Nectaris (compare Figures 9 and 10). Compositions revealed by their ejecta are mostly uniform across the extent of the mare with variations attributable to cross contamination by large impact ejecta rays and/or proximity to the basin rim. As another method for distinguishing basaltic units despite the compositional uniformity of the mare, we considered the spectral profile for each measured impact. To compensate for spurious compositional variations related to slopes and sun angle [*Jolliff*, 1999] 6 spectra were collected for each crater on the N, NE, SE, S, SW, and NW crater rim and proximal ejecta (Figure 16). These 6 points were averaged to provide a more accurate spectral profile. The crater location, size, composition, and spectra were mapped in an attempt to locate some distinctions laterally and/or vertically within Mare Nectaris.

[30] The region is complex due to the extent of crater ejecta rays that cross it. Compositional data indicate two mare basalt units, a low-Fe, low-Ti mare basalt (Iltm), and the remnants of a mid-Ti basalt (Imtm) that has not previously been described in the literature. We also mapped large-impact ejecta that are thick enough to obscure the basalt below, thus hindering a reliable assessment of the underlying basalt unit composition (Figure 13). The units are described below in order of oldest to youngest. Nomen-

clature and age relationships are based on *Wilhelms and McCauley* [1971] and *Wilhelms* [1987].

5.2.1. Unit Iltm

[31] The only correlations between crater size, location, and composition are associated with surficial features of the mare (i.e., large crater rays, proximity to basin rim) and are not due to variations in the mare composition (Figure 17). For example, data collected from our target small impacts near the basin rim have compositions between 13–14 wt% FeO and 1.5–2.5 wt% TiO_2. FeO concentrations generally increase toward the center of the mare as would be expected with increased distance from the basin rim and the influence of highland compositions. Variations from this trend are explained by the influence of large-impact ejecta rays crossing near or across the target small impacts (Figure 18). The composition of the basalts that fill Nectaris are best represented by those impacts into portions of the mare that are the least affected by ejecta rays and as far as possible from the basin rim. These crater compositions indicate that unit Iltm is 12.5–16 wt% FeO and 1.5–4 wt% TiO_2, consistent with a HA basalt composition (Figure 13).

[32] The impacts into unit Iltm reveal two different spectral profiles (Figure 16) suggesting the unit may be better depicted as two basalt units. These spectra are different from the two spectral types identified by *Kodama and Yamagucji* [2003] (Figure 15). Most of the crater spectra have a maximum absorption at 950 nm (Iltm-1), suggestive of a mineralogy dominated by clinopyroxene (cpx) (Figure 16). ~20% of the craters have maximum absorptions at 900 nm (Iltm-2), which alludes to a mineralogy dominated by lower-Ca-rich pyroxene for example, pigeonite or orthopyroxene (opx). Compositionally, Iltm-2 is intriguing in that FeO abundances may consistently exceed 14.8 wt% and TiO_2 abundances 3 wt% (Tables 3a and 3b and Figure 19). Deviations from this relationship occur only when the slope from 900 to 950 nm is virtually flat, making the peak minimum nearly indistinguishable at the spectral resolution of the Clementine camera. While the composition of Iltm-1 includes these values, the range is more varied. These two spectral profile types are randomly distributed across the mare, and are not correlated to crater size, location, or maturity. There is also no relationship between the distribution of these spectral types and basalt flow features discernible in Lunar Orbiter images. Thus we were unable to define a boundary between units Iltm-1 and Iltm-2.

[33] The relationship between the spectral profiles and FeO and TiO_2 abundances (Figure 19) have provided sufficient evidence for us to draw some conclusions regarding Unit Iltm. We interpret the broad range in compositions exhibited by Iltm-1 compared to the relatively narrow range of Iltm-2 to indicate that Iltm-2 erupted after Iltm-1, although the eruptions were probably sequential, and possibly contemporaneous. Furthermore, both FeO and TiO_2 abundances of Iltm-1 may represent the lower range in compositions of Mare Nectaris, that is 12.5–15 wt% FeO and 1.5–3 wt% TiO_2. A slightly lower FeO abundance would be associated with increased cpx (Unit Iltm-1) since Ca substitutes for Fe. The difference in mineralogy suggests the sub-units may have tapped different sources, but can also be attributed to two stages of partial melting of the same source. The first partial melt of a source would have

Table 3a. Mean Compositions and Maturity of Small Craters in Mare Nectaris Representing Sub-Unit Iltm-1

		Reflectance Spectra, nm					
FeO	TiO$_2$	415	750	900	950	1000	OMAT Number
				0.4–1 km Diameter			
12.95	2.14	0.0966	0.1593	0.1494	0.1472	0.1480	−0.880
13.76	2.06	0.0922	0.1508	0.1427	0.1401	0.1435	−0.887
15.17	2.27	0.0833	0.1371	0.1322	0.1300	0.1327	−0.908
15.06	3.05	0.0846	0.1360	0.1309	0.1291	0.1324	−0.909
10.19	1.49	0.1071	0.1719	0.1662	0.1651	0.1665	−0.913
15	3.1	0.0855	0.1366	0.1318	0.1308	0.1334	−0.917
11.83	2.27	0.0979	0.1564	0.1520	0.1508	0.1545	−0.919
14.27	2.74	0.0882	0.1405	0.1364	0.1351	0.1380	−0.920
10.36	1.83	0.1062	0.1683	0.1646	0.1632	0.1667	−0.923
15.14	3.34	0.0832	0.1329	0.1291	0.1284	0.1310	−0.926
14.66	1.92	0.0840	0.1377	0.1340	0.1334	0.1361	−0.927
12.07	1.83	0.0932	0.1533	0.1498	0.1493	0.1538	−0.930
10.82	1.26	0.0985	0.1649	0.1625	0.1611	0.1638	−0.931
14.08	3.32	0.0894	0.1431	0.1401	0.1396	0.1417	−0.933
11.8	3.08	0.1077	0.1659	0.1635	0.1625	0.1647	−0.933
15.54	2.58	0.0813	0.1310	0.1284	0.1275	0.1306	−0.934
14.36	3.13	0.0855	0.1377	0.1360	0.1346	0.1375	−0.936
10.92	1.61	0.1002	0.1622	0.1600	0.1595	0.1610	−0.938
14.75	3.31	0.0825	0.1333	0.1317	0.1305	0.1344	−0.939
10.99	1.88	0.0992	0.1595	0.1577	0.1572	0.1609	−0.941
14.63	3.82	0.0852	0.1342	0.1326	0.1317	0.1346	−0.941
16.11	4.95	0.0768	0.1227	0.1213	0.1203	0.1242	−0.942
14.86	4.07	0.0855	0.1346	0.1327	0.1324	0.1343	−0.943
14.73	3.71	0.0821	0.1319	0.1301	0.1297	0.1329	−0.943
15.79	3.64	0.0773	0.1247	0.1229	0.1225	0.1267	−0.944
14.51	2.74	0.0822	0.1347	0.1331	0.1328	0.1346	−0.945
12.8	2.38	0.0899	0.1456	0.1442	0.1439	0.1473	−0.945
10.91	1.41	0.0971	0.1599	0.1588	0.1587	0.1615	−0.947
15.19	2.92	0.0774	0.1282	0.1274	0.1267	0.1308	−0.948
15.67	3.88	0.0778	0.1250	0.1241	0.1234	0.1266	−0.949
15.35	3.22	0.0786	0.1282	0.1273	0.1268	0.1299	−0.950
10.7	1.89	0.1014	0.1644	0.1639	0.1639	0.1661	−0.951
14.41	2.89	0.0803	0.1347	0.1346	0.1336	0.1366	−0.951
15.3	3.51	0.0755	0.1219	0.1217	0.1206	0.1234	−0.951
16.04	3.98	0.0736	0.1205	0.1211	0.1207	0.1236	−0.963
				1–2 km Diameter			
13.34	3.49	0.0941	0.1430	0.1374	0.1350	0.1369	−0.903
12.68	1.76	0.0968	0.1561	0.1501	0.1484	0.1528	−0.907
14.44	2.57	0.0864	0.1405	0.1338	0.1332	0.1358	−0.907
14.59	2.71	0.0858	0.1393	0.1339	0.1321	0.1358	−0.908
13.62	2.93	0.0941	0.1476	0.1424	0.1402	0.1425	−0.908
15.62	3.27	0.0835	0.1333	0.1280	0.1265	0.1297	−0.909
11.56	1.81	0.1013	0.1628	0.1576	0.1557	0.1589	−0.911
14.99	3.62	0.0873	0.1369	0.1318	0.1303	0.1332	−0.911
14.21	3.19	0.0895	0.1417	0.1367	0.1351	0.1376	−0.912
14.62	2.68	0.0849	0.1378	0.1321	0.1315	0.1343	−0.914
12.13	2.21	0.0973	0.1550	0.1506	0.1490	0.1509	−0.917
15.3	3.3	0.0834	0.1339	0.1295	0.1282	0.1315	−0.917
15.19	3.95	0.0862	0.1350	0.1305	0.1294	0.1316	−0.918
12.92	2.18	0.0944	0.1504	0.1460	0.1449	0.1487	−0.921
14.37	3.46	0.0871	0.1381	0.1335	0.1330	0.1356	−0.922
16.1	3.52	0.0792	0.1281	0.1244	0.1232	0.1262	−0.922
14.66	3.8	0.0873	0.1372	0.1332	0.1322	0.1354	−0.923
13.55	2.12	0.0891	0.1453	0.1416	0.1403	0.1437	−0.923
13.46	2.55	0.0895	0.1437	0.1394	0.1389	0.1410	−0.925
14.06	3.52	0.0919	0.1429	0.1398	0.1383	0.1400	−0.926
15.36	3.68	0.0846	0.1356	0.1324	0.1312	0.1338	−0.927
12.68	1.69	0.0966	0.1545	0.1505	0.1501	0.1530	−0.927
14.36	3.45	0.0885	0.1385	0.1350	0.1342	0.1368	−0.928
12.26	1.88	0.0936	0.1526	0.1490	0.1484	0.1508	−0.929
15.74	3.54	0.0791	0.1270	0.1243	0.1232	0.1267	−0.931
12.92	2.19	0.0916	0.1477	0.1444	0.1439	0.1481	−0.931
11.19	2.32	0.1015	0.1630	0.1602	0.1594	0.1624	−0.932
12.29	1.84	0.0949	0.1547	0.1521	0.1511	0.1539	−0.933
15.24	3.81	0.0821	0.1311	0.1285	0.1281	0.1304	−0.937
14.81	3.22	0.0823	0.1324	0.1309	0.1301	0.1338	−0.942
13.97	2.59	0.0856	0.1393	0.1374	0.1371	0.1393	−0.942
14.7	3.15	0.0818	0.1318	0.1297	0.1296	0.1319	−0.943
14.13	2.85	0.0846	0.1368	0.1352	0.1349	0.1370	−0.945
15.03	3.24	0.0812	0.1305	0.1290	0.1286	0.1325	−0.946

Table 3a. (continued)

		Reflectance Spectra, nm					
FeO	TiO$_2$	415	750	900	950	1000	OMAT Number
13.12	1.49	0.0855	0.1440	0.1427	0.1424	0.1448	−0.947
13.71	2.17	0.0842	0.1391	0.1380	0.1375	0.1409	−0.947
14.27	2.9	0.0821	0.1333	0.1323	0.1319	0.1354	−0.949
15.54	3.96	0.0783	0.1253	0.1243	0.1243	0.1276	−0.952
14.11	2.19	0.0823	0.1348	0.1343	0.1341	0.1371	−0.954
16.55	4.3	0.0727	0.1171	0.1171	0.1167	0.1200	−0.959
			2−3 km Diameter				
12.18	1.72	0.0959	0.1579	0.1531	0.1520	0.1545	−0.918
15.24	2.54	0.0801	0.1307	0.1285	0.1273	0.1290	−0.934

higher modal cpx (provided cpx was retained in the source) compared to opx than later partial melts. The latter explanation favors two eruptions at two different times.

5.2.2. Imtm

[34] There is one region where the surface regolith slightly exceeds 5 wt% TiO$_2$ (Figure 13). There are no craters of suitable OMAT values that impact the area with which to extract information. Any compositional information from craters in or near this region have very low OMAT numbers and are compromised by prolonged space weathering. The boundary and composition of the Imtm unit is difficult to characterize because even the smallest craters expose lower FeO and TiO$_2$ abundances, compared to the surrounding regolith, as well as spectral profiles consistent with unit Iltm. If an intact unit responsible for the elevated TiO$_2$ still existed, it would be recognized by an increased FeO and/or TiO$_2$ exposed by the small impact craters.

Therefore we interpreted this area to be the remnants of a small mid-Ti flow that capped this portion of Mare Nectaris. The flow was so thin that impact gardening has virtually obliterated it as a basalt unit. Unit Imtm's original concentration of TiO$_2$ has been reduced by mixing with lower-Ti materials, yet its signature remains in the regolith (Figure 13). On the basis of the influence unit Imtm has left on the regolith, we estimated the unit has a minimum composition of 18–19 wt% FeO and 6–7 wt% TiO$_2$.

5.2.3. Units Ec, Cc$_1$, and Cc$_2$

[35] Units Ec, Cc$_1$, and Cc$_2$ are prominent crater rays and ejecta deposits that cross Nectaris contributing a significant amount of exotic material to the surface material. We defined these units by their composition, brightness, and trajectory of an ejecta ray from a know crater. The regions we analyzed are always influenced by surrounding lithologies that have contributed new regolith material since a
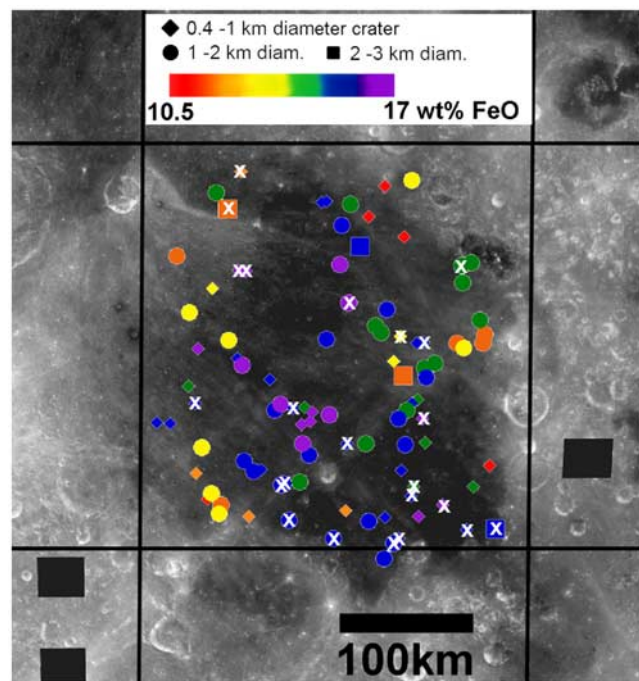
Table 3b. Mean Compositions and Maturity of Small Craters in Mare Nectaris Representing Sub-Unit Iltm-2

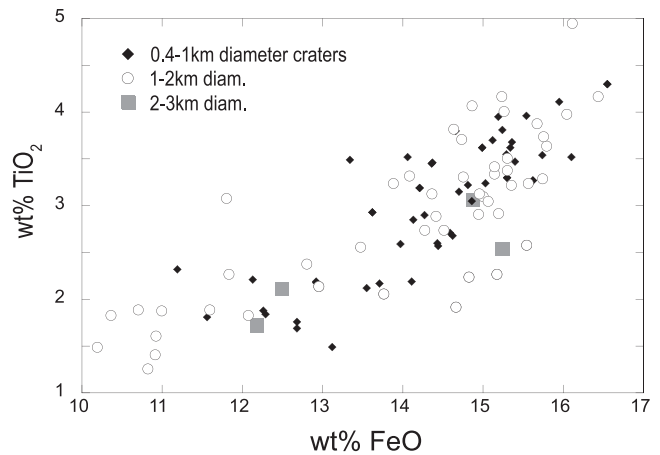|		Reflectance Spectra, nm					
FeO	TiO$_2$	415	750	900	950	1000	OMAT Number
			0.4−1 km Diameter				
15.14	3.42	0.0802	0.1303	0.1279	0.1280	0.1323	−0.942
11.59	1.89	0.0936	0.1547	0.1524	0.1527	0.1558	−0.942
15.75	3.74	0.0775	0.1251	0.1229	0.1232	0.1261	−0.946
15.26	4.01	0.0822	0.1301	0.1283	0.1284	0.1310	−0.947
14.95	3.13	0.0803	0.1311	0.1294	0.1294	0.1328	−0.947
14.82	2.24	0.0824	0.1326	0.1308	0.1310	0.1338	−0.947
15.23	4.17	0.0815	0.1299	0.1281	0.1283	0.1314	−0.948
14.94	2.91	0.0814	0.1322	0.1306	0.1307	0.1337	−0.949
13.47	2.56	0.0871	0.1411	0.1400	0.1401	0.1417	−0.951
13.88	3.24	0.0853	0.1366	0.1350	0.1357	0.1390	−0.952
16.43	4.17	0.0734	0.1184	0.1175	0.1175	0.1205	−0.954
15.56	3.24	0.0726	0.1207	0.1196	0.1202	0.1239	−0.957
15.74	3.29	0.0724	0.1204	0.1192	0.1201	0.1239	−0.960
15.3	3.38	0.0751	0.1227	0.1238	0.1251	0.1286	−0.980
			1−2 km Diameter				
15.29	3.55	0.0825	0.1319	0.1277	0.1278	0.1309	−0.929
15.34	3.62	0.0815	0.1317	0.1277	0.1280	0.1316	−0.931
15.4	3.47	0.0813	0.1313	0.1269	0.1276	0.1303	−0.932
14.75	3.71	0.0839	0.1336	0.1209	0.1309	0.1329	−0.940
14.43	2.6	0.0816	0.1329	0.1310	0.1312	0.1349	−0.947
15.12	3.7	0.0811	0.1300	0.1280	0.1284	0.1313	−0.948
15.95	4.11	0.0748	0.1206	0.1211	0.1211	0.1242	−0.966
14.86	3.05	0.0764	0.1258	0.1273	0.1284	0.1329	−0.980
			2−3 km Diameter				
12.49	2.11	0.0919	0.1483	0.1450	0.1453	0.1482	−0.937
14.87	3.06	0.0777	0.1280	0.1277	0.1288	0.1323	−0.966
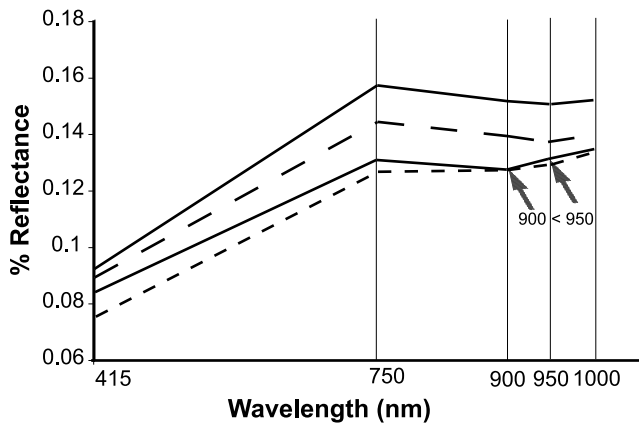
Figure 16. Spectra of selected small craters analyzed in this study that impact into unit *Iltm* in Mare Nectaris. The two top spectra are representative of most of the spectra into this unit with some increase or decrease in overall albedo. The two bottom spectra have 900 nm reflectance values less than those of the 950 nm channel.

Figure 18. Composition of rims and proximal ejecta for small impacts into Mare Nectaris. The basalts in Nectaris have a relatively uniform composition. Variations depicted in this graph are mostly due to the degree of influence of highland contamination at the site of a given impact. There appears to be no correlation between crater composition and size in Mare Nectaris. Data from Clementine 100 m/pixel at resolution.

given crater's impact event. In the case of the units described here, we felt the contamination was too extensive and may have influenced the estimate of underlying basalt unit. Several of the small-crater impact deposits into these regions gave conflicting compositions for the underlying unit with, for example, TiO_2 concentrations varying from greater than to less than the TiO_2 concentration of the surface regolith. There is no relationship with crater size, OMAT parameter, and composition, nor do the ejecta compositions describe a boundary, until the seeming ran-

domness ends, there designating the boundary of the contaminating deposits. We interpreted this phenomenon to result from heterogeneity in the volume of these obscuring deposits.

[36] Unit Ec denotes ejecta deposits from the 11 km diameter Eratosthenian crater Rosse [*Wilhelms*, 1987]. It is
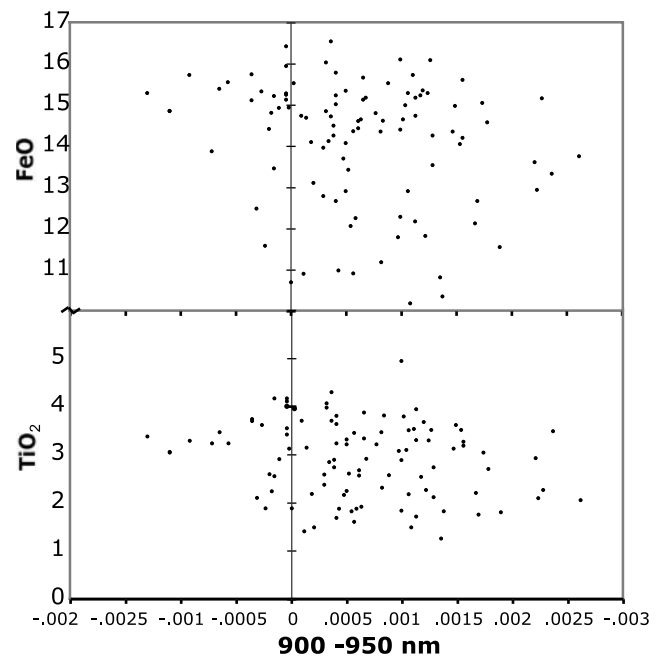

Figure 17. Location of craters from which spectral and compositional information was taken to characterize the basalt units filling Nectaris.

Figure 19. Range in FeO and TiO_2 abundances compared with the difference in the reflectance values of the 900 nm band and the 950 nm band from Clementine UV-VIS. Sub-Unit Iltm-2 is represented as negative x axis values and has a relatively narrow range in FeO and TiO_2 abundances compared with Iltm-1 (positive x axis).

younger than the mare basalts filling Nectaris, but older than other Copernican crater rays that cross it, mapped in Figure 13. Ejecta deposits classified as Cc₁ have more than one origin, as indicated by their ray trajectory, although the dominant source is probably Theophilus. Theophilus is a 100 km diameter crater of the Copernican Period in the WNW corner of Mare Nectaris, and just west of Madler (an older, late Imbrian crater) [*Wilhelms*, 1987]. Further evidence of HA basalt compositions in Mare Nectaris comes from sampled Theophilus crater ejecta by Apollo 16 [*Zeigler et al.*, 2006]. Cc₂ is the youngest crater ray to cross Nectaris originating ∼1200 km SE from the crater Tycho, which formed 109 Ma [*Wilhelms*, 1987].

6. Summary and Conclusions

[37] High-alumina mare basalts are an interesting and important part of the lunar sample collection. Their aluminous nature alludes to the depth and extent of source melting, differentiation within the lunar mantle, and to the efficiency of plagioclase separation during the crystallization of the Lunar Magma Ocean. They represent the oldest sampled mare basalts, and the return of HA basalt samples from four locations separated by ∼2400 km implies they may be widespread in both space and time on the Moon. Our research has demonstrated that HA basalts are a more common basalt type, and has broadened the surface expanse to at least 180 longitudinal degrees.

[38] One of the biggest obstacle to searching the Moon for HA basalts is that with available remote-sensing data their composition can be difficult to distinguish from the composition of a mixture of high-Fe/low-Al_2O_3 mare basalts and low-FeO/high-Al_2O_3 feldspathic highland materials. The likelihood that some or many of the HA basalts are old and thus buried by basin ejecta or younger basalt flows further exacerbates the problem. However, an assessment of the geology and actual distribution of materials with distinctive compositions at the resolution of Clementine data can be used to evaluate whether mixing produced the composition or whether a bona-fide high-Al basalt might in fact lie beneath the regolith. We have shown that FeO, TiO_2, and Th abundances, known from sample data, can be used as constraints to search the whole Moon using Lunar Prospector data. Of the regions identified in the Moon-wide search, obvious mixtures of mare and highlands are discarded by comparing remotely sensed compositional data with sample compositions. Compositional information derived from Clementine data for small craters, which expose fresh material beneath the regolith, enable an accurate assessment of basalt composition at high resolution.

[39] We have characterized the composition of the basalts that fill the Moscoviense and Nectaris basins and produced a mare basalt unit map for each. We found that Mare Moscoviense is composed of four basaltic units, two of which are HA candidates. Nectaris basin is filled by two, and possibly three basalt units. Compositional data indicates Mare Nectaris is dominated by one with a HA composition (Iltm). However, spectral profiles of the same small impacts used to extract compositional data show two mineralogies. Unit Iltm may be composed of two contemporaneous mare basalt flows, both of a HA composition. A small mid-Ti unit caps the near-center of Mare Nectaris.

[40] HA basalts in Mare Nectaris was first suggested by *Papike and Vaniman* [1978], and then by *Zeigler et al.* [2006] after their analysis of sample 60053,2-9. Our determination of HA basalts in Nectaris support their hypothesis. The discovery that the vast, and compositionally uniform Unit Iltm has two different mineralogies, yet both are still consistent with a HA basalt is supported by sample petrology of HA basalts from different regions [e.g., *Dickinson et al.*, 1985; *Dasch et al.*, 1987]. Since we have succeeded in finding HA basalts where the sample evidence points, our next endeavor is to analyze two regions from where samples were retrieved: Mare Fecunditatis and Mare Imbrium.

[41] The existence of HA basalts in the sample collection suggests that in the crystallizing LMO, a significant proportion of plagioclase remained in mare basalt source regions. Our initial search for HA basalts (Figure 3) identified their presence all over the Moon. With this evidence, one may conclude that plagioclase retention was not limited to a few isolated regions, but may have been Moon-wide. There are very few mare basalts on the lunar farside, which is attributed to the thicker crust. The validation of HA basalts existing in several of these few mare regions, as we did for Mare Moscoviense, may suggest a relationship between HA basalts and crustal thickness. Such a relationship was first suggested by [*Wilhelms*, 1987] when he wrote that the thickness of the crust beneath large basins may have influenced the composition of erupted basalts. He theorized that because of the density contrast between low- and high-Ti magmas, as well as the depth of formation of high-Al compared to low-Al magma types, low-Ti, high-Al magmas would preferentially flow into basins formed in thick crusts, such as Fecunditatis, Nectaris, and Smythii. Recent crustal thickness models [*Wieczorek and Phillips*, 1998] indicate that these basins are formed in thick crust, as well as Mare Moscoviense.

References

Albee, A. L., A. A. Chodos, A. J. Gancarz, E. L. Haines, D. A. Papanastassiou, L. Ray, F. Tera, G. J. Wasserburg, and T. Wen (1972), Mineralogy, petrology, and chemistry of Luna 16 sample b-1, *Lunar Sci.*, *III*, 10–11.

Basaltic Volcanism Study Project (1981), *Basaltic Volcanism on the Terrestrial Planets*, 1286 pp., Pergamon, New York.

Beaty, D. W., S. M. R. Hill, A. L. Albee, and W. S. Baldridge (1979), Apollo 12 feldspathic basalts 12031, 12038, and 12072: Petrology, comparison, and interpretation, *Proc. Lunar Planet. Sci. Conf. 10th*, 115–139.

Brunfelt, A. O., K. S. Heier, B. Nilssen, B. Sundvoll, and E. Steinnes (1972a), Distribution of elements between different phases of Apollo 14 rocks and soils, *Proc. Lunar Sci. Conf. 3rd*, 1133–1147.

Brunfelt, A. O., K. S. Heier, and E. Steinnes (1972b), Distribution of elements between different phases of Apollo 14 rocks and soils, *Proc. Lunar Sci. Conf. 2nd*, 1133–1147.

Burns, R. G. (1982), *Mineralogical Applications of Crystal Field Theory*, 2nd ed., 551 pp., Cambridge Univ. Press, New York.

Cadogen, P. H., and G. Turner (1977), ^{40}Ar-^{39}Ar dating of Luna 16 and Luna 20 samples, *Philos. Trans. R. Soc. London, Ser. A*, *284*, 167–177.

Charette, M. P., T. B. McCord, and C. Pieters (1974), Application of remote spectral reflectance measurements to lunar geology classification and

determination of titanium content of lunar soils, *J. Geophys. Res.*, *79*, 1605–1613.

Cohen, B. A., G. A. Snyder, C. M. Hall, L. A. Taylor, and M. A. Nazarov (2001), Argon-40-argon-39 chronology and petrogenesis along the eastern limb of the Moon from Luna 16, 20, and 24 samples, *Meteorit. Planet. Sci.*, *36*, 1345–1366.

Craddock, R. A., M. S. Robinson, B. R. Hawke, and A. S. McEwen (1997), Clementine-based geology of the Moscoviense basin, lunar farside (abstract), *Lunar Planet. Sci.*, *XXVIII*, 265–266.

Dasch, E. J., C. Y. Shih, B. M. Bansal, H. Weismann, and L. E. Nyquist (1987), Isotopic analysis of basaltic fragments from lunar breccia 14321: Chronology and petrogenesis of pre-imbrium mare volcanism, *Geochim. Cosmochim. Acta*, *51*, 3241–3254.

Dickinson, T., G. J. Taylor, K. Keil, R. A. Schmitt, S. S. Hughes, and M. R. Smith (1985), Apollo 14 aluminous mare basalts and their possible relationship to KREEP, *J. Geophys. Res.*, *90*, C365–C375.

Duncan, A. R., S. M. McKay, J. W. Stoeser, M. M. Lindstrom, D. J. Lindstrom, J. S. Fructher, and G. G. Goles (1975), Lunar polymict breccia 14321: A compositional study of its principle components, *Geochim. Cosmochim. Acta*, *39*, 247–260.

Ehmann, W. D., D. E. Gillum, and J. W. Morgan (1972), Oxygen and bulk elemental composition studies of Apollo 14 and other lunar rocks and soils, *Geochim. Cosmochim. Acta*, *2*, 1149–1160.

El Goresy, A., P. Ramdohr, and L. A. Taylor (1972), Fra Mauro crystalline rocks: Petrology, geochemistry, and subsolidus reduction of the opaque minerals (abstract), *Lunar Sci.*, *III*, 224–226.

Eliason, E. M. (1997), Production of digital image models using the ISIS system (abstract), *Lunar Planet. Sci.*, *XXVII*, 331–332.

Eliason, E. M. (1999), Digital processing for a global multispectral map of the Moon from the Clementine UVVIS imaging instrument, *Lunar Planet. Sci.*, *XXX*, Abstract 1933.

Feldman, W. C., B. L. Barraclough, K. R. Fuller, D. J. Lawrence, S. Maurice, M. C. Miller, T. H. Prettyman, and A. B. Binder (1999), The Lunar Prospector gamma-ray and neutron spectrometers, *Nucl. Instrum. Methods Phys. Res., Sect. A*, *422*, 562–566.

Fernandes, V. A., R. Burgess, and G. Turner (2000), Laser argon-40-argon-39 age studies of Dar al Gani 262 meteorite, *Meteorit. Planet. Sci.*, *35*, 1355–1364.

Fischer, E. M., and C. M. Pieters (1994), Remote determination of exposure degree and iron concentration of lunar soils using VIS-NIR spectroscopic methods, *Icarus*, *111*, 475–488.

Fischer, E. M., and C. M. Pieters (1996), Composition and exposure age of the Apollo 16 Cayley and Descartes regions from Clementine data: Normalizing the optical effects of space weathering, *J. Geophys. Res.*, *101*(E1), 2225–2234.

Gillis, J. J. (1998), The composition and geologic setting of mare deposits on the far side of the Moon, Ph.D. thesis, Rice Univ., Houston, Tex.

Gillis, J. J., and P. D. Spudis (2000), Geology of the Smythii and Marginis region of the Moon: Using integrated remotely sensed data, *J. Geophys. Res.*, *105*(E2), 4217–4233.

Gillis, J. J., B. L. Jolliff, and R. C. Elphic (2003), A revised algorithm for calculating TiO_2 from Clementine UVVIS data: A synthesis of rock, soil, and remotely sensed TiO_2 concentrations, *J. Geophys. Res.*, *108*(E2), 5009, doi:10.1029/2001JE001515.

Gillis, J. J., B. L. Jolliff, and R. L. Korotev (2004), Lunar surface geochemistry: Global concentrations of Th, K, and FeO as derived from Lunar Prospector and Clementine data, *Geochim. Cosmochim. Acta*, *68*(18), 3791–3805.

Grieve, R. A. F., G. A. McKay, and D. F. Weill (1972), Microprobe studies of three Luna 16 basalt fragments, *Earth Planet. Sci. Lett.*, *13*, 233–242.

Grieve, R. A. F., G. A. McKay, H. D. Smith, and D. F. Weill (1975), Lunar polymict breccia 14321: A petrographic study, *Geochim. Cosmochim. Acta*, *39*, 229–246.

Hawke, B. R., P. G. Lucey, G. A. Smith, G. J. Taylor, D. J. Lawrence, and P. D. Spudis (2001), Remote sensing studies of selected spectral anomalies on the Moon, *Lunar Planet. Sci.*, *XXXII*, Abstract 1241.

Hawke, B. R., J. J. Gillis, T. A. Giguere, D. T. Blewett, D. J. Lawrence, P. G. Lucey, G. A. Smith, P. D. Spudis, and G. J. Taylor (2005a), Remote sensing and geologic studies of the Balmer-Kapteyn region of the Moon, *J. Geophys. Res.*, *110*, E06004, doi:10.1029/2004JE002383.

Hawke, B. R., et al. (2005b), The earliest mare basalts, *Lunar Planet. Sci.*, *XXXVI*, Abstract 1642.

Helmke, P. A., and L. A. Haskin (1972), Rare earths and other trace elements in Luna 16 soil, *Earth Planet. Sci. Lett.*, *13*, 441–443.

Hiesinger, H., R. Jaumann, G. Neukum, and J. W. Head (1996), Mare Australe: New results from Lunar Orbiter and Clementine UV/VIS imagery (abstract), *Lunar Planet. Sci.*, *XXVII*, Part 2, 545–546.

Hubbard, N. J., P. W. Gast, J. M. Rhodes, B. M. Bansal, and H. Weismann (1972a), Nonmare basalts: Part II, *Geochim. Cosmochim. Acta*, *2*, 1161–1179.

Hubbard, N. J., L. E. Nyquist, J. M. Rhodes, B. M. Bansal, H. Wiesman, and S. E. Church (1972b), Chemical features of the Luna 16 regolith sample, *Earth Planet. Sci. Lett.*, *13*, 423–428.

Huneke, J. C., F. A. Podosek, and G. J. Wasserburg (1972), Gas retention and cosmic-ray exposure ages of a basalt fragment from Mare Fecunditatis, *Earth Planet. Sci. Lett.*, *13*, 375–383.

Jakes, P., J. Warner, W. I. Ridley, A. M. Reid, R. S. Harmon, R. Brett, and R. W. Brown (1972), Petrology of a portion of the Mare Fecunditatis regolith, *Earth Planet. Sci. Lett.*, *13*, 257–271.

Jolliff, B. L. (1999), Clementine UVVIS multispectral data and the Apollo 17 landing site: What can we tell and how well?, *J. Geophys. Res.*, *104*(E6), 14,123–14,148.

Jolliff, B. L., J. J. Gillis, L. A. Haskin, and R. L. Korotev (2000), Major lunar crustal terranes: Surface expressions and crust-mantle origins, *J. Geophys. Res.*, *105*(E2), 4197–4216.

Kodama, S., and Y. Yamagucji (2003), Lunar mare volcanism in the eastern nearside region derived from Clementine UV/VIS data, *Meteorit. Planet. Sci.*, *38*(10), 1461–1484.

Kurat, G., A. Kracher, K. Keil, R. Warner, and M. Prinz (1976), Composition and origin of Luna 16 aluminous mare basalts, *Proc. Lunar Sci. Conf. 7th*, Part 2, 1301–1321.

Lawrence, D. J., W. C. Feldman, B. L. Barraclough, A. B. Binder, R. C. Elphic, S. Maurice, and D. R. Thomsen (1998), Global elemental maps of the Moon: The Lunar Prospector gamma-ray spectrometer, *Science*, *281*, 1484–1489.

Lawrence, D. J., W. C. Feldman, R. C. Elphic, S. Maurice, T. H. Prettyman, and A. B. Binder (2003), Iron abundances on the lunar surface as measured by the Lunar Prospector Gamma-Ray Spectrometer, *Lunar Planet. Sci.*, *XXXII*, Abstract 1830.

Li, L., and J. F. Mustard (2000), Compositional gradients across mare-highland contacts: Importance and geological implication of lateral transport, *J. Geophys. Res.*, *105*(E8), 20,431–20,450.

Li, L., and J. F. Mustard (2003), Highland contamination in lunar mare soils: Improved mapping with multiple end-member spectral mixture analysis (MESMA), *J. Geophys. Res.*, *108*(E6), 5053, doi:10.1029/2002JE001917.

Lindstrom, M. M., A. R. Duncan, J. S. Fruchter, S. M. McKay, J. W. Stoeser, G. G. Goles, and D. J. Lindstrom (1972), Compositional characteristics of some Apollo 14 clastic materials, *Geochim. Cosmochim. Acta*, *2*, 1201–1214.

Longhi, J., D. Walker, and J. Hays (1972), Petrography and crystallization history of basalts 14310 and 14,072, *Proc. Lunar Sci. Conf. 3rd*, Part 2, 131–139.

Lucey, P. G., D. T. Blewett, and B. R. Hawke (2000a), Lunar iron and titanium abundance algorithms based on final processing of Clementine ultraviolet-visible images, *J. Geophys. Res.*, *105*(E8), 20,297–20,305.

Lucey, P. G., D. T. Blewett, and B. R. Hawke (2000b), Imaging of lunar surface maturity, *J. Geophys. Res.*, *105*(E8), 20,377–20,386.

Ma, M. S., R. A. Schmitt, R. L. Nielsen, G. J. Taylor, R. D. Warner, and K. Keil (1979), Petrogenesis of Luna 16 aluminous mare basalts, *Geophys. Res. Lett.*, *6*, 909–912.

McCord, T. B., and J. B. Adams (1973), Progress in remote optical analysis of lunar surface composition, *Moon*, *7*, 453–474.

McKay, D. S., G. H. Heiken, A. Basu, G. Blanford, S. Simon, R. Reedy, B. M. French, and J. Papike (1991), The Lunar Regolith, in *Lunar Sourcebook*, pp. 285–356, Cambridge Univ. Press, New York.

Melosh, H. J. (1989), *Impact Cratering: A Geologic Process*, 245 pp., Oxford Univ. Press, New York.

Merenyi, E., A. S. McEwen, M. S. Robinson, and R. A. Craddock (1997), Spectral mapping of Mare Moscoviense, lunar farside, from Clementine UVVIS data (abstract), *Lunar Planet. Sci.*, *XXVIII*, 939–940.

Mustard, J. F., and J. W. Head (1996), Buried stratigraphic relationships along the southwestern shores of Oceanus Procellarum: Implications for early lunar volcanism, *J. Geophys. Res.*, *101*, 18,913–18,925.

Neal, C. R., and G. Y. Kramer (2006), The petrogenesis of the Apollo 14 high-Al mare basalts, *Am. Mineral.*, *91*, 1521–1535.

Neal, C. R., and L. A. Taylor (1989), Metasomatic products of the lunar magma ocean: The role of KREEP dissemination, *Geochim. Cosmochim. Acta*, *53*, 529–541.

Neal, C. R., L. A. Taylor, and M. M. Lindstrom (1988), Apollo 14 mare basalt petrogenesis: Assimilation of KREEP-like components by a factionating magma, *Proc. Lunar Planet. Sci. Conf. 18th*, 139–153.

Neal, C. R., L. A. Taylor, and A. D. Patchen (1989), High alumina (HA) and very high potassium (VHK) basalt clasts from Apollo 14 breccias, part 1: Mineralogy and petrology: Evidence of crystallization from evolving magmas, *Proc. Lunar Planet. Sci. Conf. 19th*, 137–145.

Neal, C. R., M. D. Hacker, G. A. Snyder, L. A. Taylor, Y. G. Liu, and R. A. Schmitt (1994), Basalt generation at the Apollo 12 site, part 2: Source heterogeneity, multiple melts, and crustal contamination, *Meteoritics*, *2*, 349–361.

Nozette, S., et al. (1994), The Clementine mission to the Moon: Scientific overview, *Science*, *266*, 1835–1839.

Nyquist, L. E., and C. Y. Shih (1992), The isotopic record of lunar volcanism, *Geochim. Cosmochim. Acta*, *56*, 2213–2234.

Nyquist, L. E., J. L. Wooden, C. Y. Shih, H. Wiesmann, and B. M. Bansal (1981), Isotopic and REE studies of lunar basalt 12038: Implications for petrogenesis of aluminous basalts, *Earth Planet. Sci. Lett.*, *55*, 335–355.

Papanastassiou, D. A., and G. A. Wasserburg (1971), Rb-Sr ages of the igneous rocks from the Apollo 14 mission and the age of the Fra Mauro Formation, *Earth Planet. Sci. Lett.*, *12*, 36–48.

Papike, J. J., and D. T. Vaniman (1978), The lunar mare basalt suite, *Geophys. Res. Lett.*, *5*(6), 433–436.

Papike, J. J., A. E. Bence, and D. H. Lindsley (1974), Mare basalts from the Taurus-Littrow region of the Moon, *Proc. Lunar Sci. Conf.*, *5th*, 471–504.

Papike, J. J., G. Ryder, and C. K. Shearer (1998), Lunar samples, in *Planetary Materials*, pp. 5–234, Mineral. Soc. of Am., Washington, D. C.

Pieters, C. M. (1978), Mare basalt types on the front side of the Moon: A summary of spectral reflectance data, *Proc. Lunar Planet. Sci. Conf. 9th*, 2825–2849.

Pieters, C. M., G. He, S. Tompkins, M. I. Staid, and E. M. Fischer (1995), The low-Ti basalts of Tsiolkovsky as seen by Clementine, *Lunar Planet. Sci.*, *XXVI*, 1121–1122.

Prettyman, T. H., W. C. Feldman, D. J. Lawrence, G. W. McKinney, A. B. Binder, R. C. Elphic, O. M. Gasnault, S. Maurice, and K. R. Moore (2002), Library least squares analysis of Lunar Prospector gamma-ray spectra, *Lunar Planet. Sci.*, *XXXIII*, Abstract 2012.

Reid, A., and P. Jakes (1974), Luna 16 revisited: The case for aluminous mare basalts (abstract), *Lunar Sci.*, *13*(2), 627–629.

Reid, A., G. J. Taylor, U. B. Marvin, and W. J. A (1972), Luna 16: Relative proportions and petrologic significance of particles in the soil from Mare Fecunditatis, *Earth Planet. Sci. Lett.*, *13*, 286–298.

Ridley, W. I. (1975), On high-alumina mare basalts, *Proc. Lunar Sci. Conf.*, *6th*, 131–145.

Shearer, C. K., and J. J. Papike (1999), Magmatic evolution of the Moon, *Am. Mineral.*, *84*, 1469–1494.

Shervais, J. W., L. A. Taylor, and M. M. Lindstrom (1985), Apollo 14 mare basalts: Petrology and geochemistry of clasts from consortium breccia 14321, *Proc. Lunar Planet. Sci. Conf. 15th*, Part 2, *J. Geophys. Res.*, *90*, suppl., C375–C395.

Shih, C. Y., and L. E. Nyquist (1989a), Isotopic and chemical constraints on models of aluminous mare basalts genesis (abstract), *Lunar Planet. Sci.*, *XX*, 1002–1003.

Shih, C. Y., and L. E. Nyquist (1989b), Isotopic constraints on the petrogenesis of Apollo 14 igneous rocks, in *Workshop on Moon in Transition: Apollo 14, KREEP, and Evolved Lunar Rocks*, *LPI Tech. Rep. 89-03*, edited by G. J. Taylor and P. H. Warren, p. 128, Lunar and Planet. Inst., Houston, Tex.

Shkuratov, Y. G., V. G. Kaydash, and N. V. Opanasenko (1999), Iron and titanium abundances and maturity degree distribution on the lunar nearside, *Icarus*, *137*(2), 222–234.

Snyder, G. A., L. A. Taylor, and C. R. Neal (1992), A chemical model for generating the sources of mare basalts: Combined equilibrium and fractional crystallization of the lunar magmasphere, *Geochim. Cosmochim. Acta*, *56*, 3809–3823.

Snyder, G. A., L. E. Borg, L. E. Nyquist, and L. A. Taylor (2000), Chronology and isotopic constraints on lunar evolution, in *Origin of Earth and Moon*, edited by R. M. Canup and K. Righter, pp. 361–395, Lunar and Planet. Inst., Houston.

Staid, M. I., and C. M. Pieters (2000), Integrated spectral analysis of mare soils and craters: Application to eastern nearside basalts, *Icarus*, *145*, 122–139.

Staid, M. I., C. M. Pieters, and J. W. Head (1996), Mare Tranquillitatis: Basalt emplacement history and relation to lunar samples, *J. Geophys. Res.*, *101*, 23,313–23,228.

Strasheim, A., P. F. S. Jackson, J. H. J. Coetzee, F. W. E. Strelow, F. T. Wybenga, A. J. Gricius, M. L. Kokot, and R. H. Scott (1972), Analysis of lunar samples 14163, 14259, and 14321 with isotopic data for $^7Li/^6Li$, *Geochim. Cosmochim. Acta*, *2*, 1337–1342.

Taylor, G. J., P. Warren, G. Ryder, J. Delano, C. Pieters, and G. Lofgren (1991), Lunar rocks, in *Lunar Sourcebook*, edited by G. H. Heiken, D. T. Vaniman, and B. M. French, pp. 183–284, Cambridge Univ. Press, New York.

Taylor, L. A., J. W. Shervais, R. B. Hunter, C. Y. Shih, B. M. Bansal, J. Wooden, L. E. Nyquist, and L. C. Laul (1983), Pre-4.2 AE mare basalt volcanism in the lunar highlands, *Earth Planet. Sci. Lett.*, *66*, 33–47.

Taylor, L. A., C. M. Pieters, L. P. Keller, R. V. Morris, and D. S. McKay (2001), Lunar mare soils: Space weathering and the major effects of surface-correlated nanophase Fe, *J. Geophys. Res.*, *106*(E11), 27,985–27,999.

Taylor, S. R., and P. Jakes (1974), The geochemical evolution of the Moon, *Proc. Lunar Sci. Conf. 5th*, 1287–1305.

Taylor, S. R., M. Kaye, P. Muir, W. Nance, R. Rudowski, and N. Ware (1972), Composition of the lunar uplands: Chemistry of Apollo 14 samples from Fra Mauro, *Proc. Lunar Sci. Conf.*, *3rd*, 1231–1249.

Wieczorek, M. A., and R. J. Phillips (1998), Potential anomalies on a sphere: Applications to the thickness of the lunar crust, *J. Geophys. Res.*, *103*(E1), 1715–1724.

Wilcox, B. B., P. G. Lucey, and J. J. Gillis (2005), Mapping iron in the lunar mare: An improved approach, *J. Geophys. Res.*, *110*, E11001, doi:10.1029/2005JE002512.

Wilhelms, D. (1987), *The Geologic History of the Moon*, U.S. Geol. Surv. Prof., 1348.

Wilhelms, D. E., and J. F. McCauley (1971), Geologic map of the near side of the Moon, *U.S. Geol. Surv. Misc. Invest. Ser.*, Map I-703.

Zeigler, R. A., L. A. Korotev, R. L. Haskin, B. L. Jolliff, and J. J. Gillis (2006), Petrography and geochemistry of five new Apollo 16 mare basalts and evidence for post-basin deposition of basaltic material at the site, *Meteorit. Planet. Sci.*, *41*(2), 263–284.

————————————

B. L. Jolliff, Department of Earth and Planetary Sciences, Washington University, Campus Box 1169, One Brookings Drive, St. Louis, MO 63130, USA.

G. Y. Kramer, Bear Fight Center, 22 Fiddler's Road, Winthrop, WA 98862, USA. (gkramer@bearfightcenter.com)

C. R. Neal, Department of Civil Engineering and Geological Sciences, University of Notre Dame, Notre Dame, IN 46556, USA.